SIAM J. APPL. MATH.
Vol. 78, No. 3, pp. 1300–1329

UPSCALING DIFFUSION THROUGH FIRST-ORDER VOLUMETRIC SINKS: A HOMOGENIZATION OF BACTERIAL NUTRIENT UPTAKE*

MOHIT P. DALWADI†, YANMING WANG†, JOHN R. KING‡, AND NIGEL P. MINTON†

Abstract. In mathematical models that include nutrient delivery to bacteria, it is prohibitively expensive to include a pointwise nutrient uptake within small bacterial regions over bioreactor length-scales, and so such models often impose an effective uptake instead. In this paper, we systematically investigate how the effective uptake should scale with bacterial size and other microscale properties under first-order uptake kinetics. We homogenize the unsteady problem of nutrient diffusing through a locally periodic array of spherical bacteria, within which it is absorbed. We introduce a general model that could also be applied to other single-cell microorganisms, such as cyanobacteria, microalgae, protozoa, and yeast, and we consider generalizations to arbitrary bacterial shapes, including some analytic results for ellipsoidal bacteria. We explore in detail the three distinguished limits of the system on the timescale of diffusion over the macroscale. When the bacterial size is of the same order as the distance between them, the effective uptake has two limiting behaviors, scaling with the bacterial volume for weak uptake and with the bacterial surface area for strong uptake. We derive the function that smoothly transitions between these two behaviors as the system parameters vary. Additionally, we explore the distinguished limit in which bacteria are much smaller than the distance between them and have a very strong uptake. In this limit, we find that the effective uptake is bounded above as the uptake rate grows without bound; we are able to quantify this and characterize the transition to the other limits we consider.

Key words. bacterial uptake, multiscale, distinguished limits, effective uptake

AMS subject classifications. 35B27, 35K57, 80A30, 92C45

DOI. 10.1137/17M1138625

1. Introduction.

As the technology to manipulate the metabolic pathways of microorganisms grows more sophisticated, more chemicals become industrially viable targets for biosynthetic production. For example, microorganisms can be used as "cell factories" to produce environmentally friendly biofuels, cheaper medicines, and fine chemicals [20]. In order to control and optimize the industrial production of such chemicals, it is important to understand how nutrient is transported to and absorbed by these microorganisms.

A typical experimental set-up for a cell factory involves feeding bacteria with nutrient within a liquid-filled bioreactor. As bacterial movement is generally forced by the fluid flow in these bioreactors, there is little relative advection close to each bacterium. Thus, the nutrient absorbed by the bacteria causes a concentration gradient close to the bacteria that drives further nutrient toward the bacteria. While the mathematical equations that govern the salient transport processes such as dif-

*Received by the editors July 13, 2017; accepted for publication (in revised form) February 21, 2018; published electronically May 3, 2018. The data in this paper are available from https://doi.org/10.17639/nott.348.

http://www.siam.org/journals/siap/78-3/M113862.html

Funding: This work was supported by the Biotechnology and Biological Sciences Research Council [grant number BB/L013940/1]; and the Engineering and Physical Sciences Research Council, jointly funding the first grant number.

†Synthetic Biology Research Centre, University of Nottingham, University Park, Nottingham, NG7 2RD, UK (mohit.dalwadi@nottingham.ac.uk, yanming.wang@nottingham.ac.uk, nigel.minton@nottingham.ac.uk).

‡School of Mathematical Sciences, University of Nottingham, University Park, Nottingham, NG7 2RD, UK (john.king@nottingham.ac.uk).

fusion, advection, and chemical reaction are well known [4], there is a considerable separation between the longer bioreactor (0.1–1 m) and shorter bacterial (0.1–10 μm) lengthscales [21], which we refer to as the macroscale and microscale, respectively. Hence, it is prohibitively expensive to include bacterial regions in a computational model of bacterial uptake over the length of a bioreactor.

One method to bypass this expense is to treat the liquid and bacterial regions as a single-phase domain, and to model the bacterial uptake as an effective nutrient sink over this domain. While this is a computationally efficient resolution, it is not immediately clear how to relate properties on the bacterial scale, such as bacterial size and kinetic uptake parameters, with this effective result. For example, one may intuitively expect the effective uptake to scale with bacterial volume for weak uptake and to scale with bacterial surface area for strong uptake. Our goal in this paper is to quantify when each of these scalings is valid, obtain the correct form of the effective uptake when neither is appropriate, and characterize the smooth transition between these canonical forms of the effective uptake as a function of the system parameters.

To investigate these questions, we systematically upscale the microscale problem of unsteady diffusion through and past a locally periodic array of spherical bacteria that act as volume sinks of nutrient with first-order kinetics, governed by the reaction–diffusion equation

$$\frac{\partial c}{\partial t} = \nabla \cdot (\tilde{D}\nabla c) - \tilde{\lambda} c, \tag{1}$$

with continuous concentration and flux across the bacterial membrane, with set-up shown in Figure 1. Here, $\tilde{D}$ and $\tilde{\lambda}$ are piecewise-constant functions which are discontinuous across each bacterial membrane, and where $\tilde{\lambda}$ vanishes outside each bacteria. Our main goal is to determine the effective uptake of the upscaled system in the distinguished limits where the effective uptake balances the macroscale diffusion, in particular when $\tilde{D}$ and $\tilde{\lambda}$ depend on the separation distance between bacteria. To focus on the competing effects of diffusion and uptake, we do not consider advection in this problem. We show that when the effective uptake balances the macroscale diffusion over the timescale of the latter, the inclusion of just diffusion and uptake can lead to three distinguished asymptotic limits, which we comprehensively analyze. Investigating these three distinguished limits allows us to characterize the upscaled problem for general single-celled microorganisms, including cyanobacteria, microalgae, protozoa, and yeast, for which different parameter regimes may be appropriate. To upscale this problem, we use mathematical homogenization (as outlined in, for example, [3, 27, 17]) via the method of multiple scales (also known as periodic homogenization) rather than, for example, volume averaging methods [32]. We note that, in practice, both methods result in the same averaged equations [12].

One of the asymptotic limits we consider in this paper is a double-porosity model [1], where a coefficient (often the porosity or diffusion coefficient) varies greatly between two regions and is a function of the small parameter of periodicity. A notable property of double-porosity models is that the upscaled equations often exhibit a memory effect—that is, in averaging the problem from a time-local microscale problem up to a macroscale problem, the history of the problem becomes important, and this can cause a partial differential equation to be upscaled into an integrodifferential equation [24], as we shall encounter in this paper. This effect is equivalent to having coupled partial differential equations to solve on the macroscale, as the equations cannot be solved one after the other but rather must be solved simultaneously (disregarding iterative methods).

Another asymptotic limit we consider in this paper is that of very small bacteria, i.e., when the bacterial radius is much smaller than the distance between sphere centers. In such problems, there may be a critical size of the inner problem for which a distinguished limit arises. In [8] (see [23] for the original in French), the homogenization of Laplace's equation in an n-dimensional domain periodically perforated with n-dimensional spheres is considered, and in the three-dimensional case the critical perforation size is identified as being proportional to the cube of the small parameter of periodicity. In this paper, we investigate the distinguished limit in which the bacterial size has the same critical scaling as these cases, combined with a very large uptake coefficient. We homogenize this case in a manner similar to that in [6], where the authors use the method of matched asymptotic expansions within a homogenization procedure to calculate an effective boundary condition for the shielding of a Faraday cage. In contrast to the perforated domain cases mentioned above, in this paper we must also solve a problem within each bacterium.

There has been previous work homogenizing solute transport problems with adsorption or chemical reaction within disconnected periodic subdomains of the full domain, and we next discuss several notable examples of particular relevance to this paper. In [18], the authors consider Stokes flow coupled with an advection–diffusion solute transport problem past a periodic array of permeable obstacles. The solute can diffuse within the obstacle, and there are general nonlinear reaction terms in both the fluid and obstacle phases. The solute concentrations in these phases are coupled via continuity of mass flux and one of six different additional conditions. The diffusion coefficient within the obstacle phase is much smaller than the diffusion coefficient within the fluid phase, yielding a double-porosity model that results in a memory term in the homogenized equation. In [9], the authors consider steady diffusion with local forcing past a periodic array of obstacles for two cases; the second of these is relevant for our work and involves diffusion and nonlinear uptake within the obstacles, coupled via continuity of concentration and concentration flux on the surface of the obstacles. The diffusion coefficients inside and outside the obstacles are of the same order. In [28], Navier–Stokes flow in capillaries is coupled to Darcy flow in tissue, and these both feed into an advection–diffusion equation for drug transport through both phases, with a linear uptake term within the tissue, all in a periodic domain. The flow equations are upscaled in the double-porosity limit, and the drug transport equations are upscaled for several different coupling conditions, with a focus on advective transport. In [15], the authors consider diffusive transport with nonlinear reaction terms in a periodic domain containing a multiply connected subdomain with different diffusion coefficient and reaction terms from the rest of the domain. At the interface between these regions, the fluxes are general nonlinear functions of the concentrations on either side of the interface.

In each of the papers discussed in the above paragraph, the structure of the periodic microscale is fairly general, allowing for homogenized equations to be calculated in terms of general cell problems. While this generality is valuable, it also means that effective terms are not calculated explicitly. Thus, the generality of these problems is not conducive to a systematic investigation of how the effective parameters vary as a function of the system parameters.

We mainly consider spherical bacteria (*cocci*), whose radius can vary slowly over the macroscale, but also consider the generalization to arbitrary bacterial shapes in Appendix A, including some analytic results for ellipsoidal bacteria. Traditional homogenization techniques require a strictly periodic microscale geometry, but there are methods to extend these techniques to problems with a microscale that varies over the

macroscale [30, 26, 5]. These extensions have formal roots in [2] and [7], and there has been a significant amount of recent applied work on homogenizing specific problems involving reaction and diffusion processes, such as [14, 25]. The key idea behind extending standard homogenization theory from a strictly periodic microstructure to a locally periodic microstructure is to use a level-set function in both the microscale and macroscale variables to define the microstructure [31]. Consequently, this extension is sometimes referred to as the level-set framework. In general, this method requires a different cell problem to be solved at every point in the macroscale rather than just once for the entire problem (as is the case for standard homogenization theory), but this additional computational expense can be bypassed by imposing a specific one-parameter shape on the microstructure [5, 10]. This is the route we take in the main text of this paper; restricting our main analysis to spherical bacteria allows us to maximize our analytic progress and, consequently, to systematically analyze the form of the effective uptake in the three distinguished limits we consider, yielding greater physical insight into the system behavior as a function of the system parameters. Additionally, and to the same end, we neglect any internal structure of the bacteria, treating the bacterial interior as homogeneous. Finally, we note that, in this paper, we only use "cell" in the language of mathematical homogenization and never in the biological sense; that is, we only use "cell" to refer to the periodic unit cell domain in what is commonly referred to as a "cell problem" in mathematical homogenization.

The structure of this paper is as follows. We present a dimensional description of the bacterial uptake model in section 2 and form the dimensionless problem. We then formulate the problem to be upscaled via homogenization theory in section 3 and upscale this problem for three distinguished limits in sections 3.1, 3.2, and 3.3. We briefly consider the generalization of these results to arbitrary bacterial shapes in Appendix A, including some analytic results for ellipsoidal bacteria in one sublimit. Finally, we discuss the physical implications of these results and conclude in section 4.

2. Model description. We consider the diffusion and uptake of nutrient through a colony of bacteria within a passive medium, which could model fluid within a bioreactor or the extracellular polymeric substance within a biofilm. We describe the nutrient distribution in terms of its concentration, which is defined in the medium and bacterial phases as $\tilde{c}(\tilde{\boldsymbol{x}},\tilde{t})$ and $\tilde{C}(\tilde{\boldsymbol{x}},\tilde{t})$, respectively. Here, $\tilde{c}$ and $\tilde{C}$ are given in terms of the molarity of the concentration, $\tilde{\boldsymbol{x}}$ is the spatial vector coordinate, and $\tilde{t}$ is time. We assume that the nutrient diffuses through the passive medium with constant diffusion coefficient D_m, and through the bacteria with constant diffusion coefficient D_b. Additionally, we assume that the nutrient uptake occurs only within the bacteria, and that the uptake is proportional to the nutrient concentration with rate of proportionality λ.

We model the bacteria as a collection of spheres whose centers are located on a cubic lattice at a distance ϵl apart, where ϵ is a small dimensionless parameter and l is the typical length of the entire domain. The radii of the bacteria can vary slowly in space, and a bacterium centered at $\tilde{\boldsymbol{x}}$ has radius $\tilde{R}(\tilde{\boldsymbol{x}})$. For simplicity, we retain a fixed cell size. We only consider nonoverlapping spheres, and thus $2\tilde{R} < \epsilon l$. The bacterial and medium phases are denoted as $\Omega_b \subset \mathbb{R}^3$ and $\Omega_m \subset \mathbb{R}^3$, respectively. We denote the entire spatial domain as $\Omega = \Omega_b \cup \Omega_m \subset \mathbb{R}^3$ and note that $\Omega_b \cap \Omega_m = \emptyset$. Finally, we also denote the boundary between the two phases as $\partial\Omega_b$, which we refer to as the "bacterial membrane" or just "membrane." To couple the concentrations across the bacterial membrane, we assume continuity of concentration and concentration flux.

Mathematically, we have the dimensional problem

$$\frac{\partial \tilde{c}}{\partial \tilde{t}} = D_m \nabla^2 \tilde{c} \quad \text{for } \tilde{\boldsymbol{x}} \in \Omega_m, \tag{2a}$$

$$\frac{\partial \tilde{C}}{\partial \tilde{t}} = D_b \nabla^2 \tilde{C} - \lambda \tilde{C} \quad \text{for } \tilde{\boldsymbol{x}} \in \Omega_b, \tag{2b}$$

$$\tilde{c} = \tilde{C} \quad \text{for } \tilde{\boldsymbol{x}} \in \partial\Omega_b, \tag{2c}$$

$$\boldsymbol{n} \cdot D_m \nabla \tilde{c} = \boldsymbol{n} \cdot D_b \nabla \tilde{C} \quad \text{for } \tilde{\boldsymbol{x}} \in \partial\Omega_b, \tag{2d}$$

$$\tilde{c}(\tilde{\boldsymbol{x}}, 0) = \tilde{c}_{\text{init}}(\tilde{\boldsymbol{x}}) \quad \text{for } \tilde{\boldsymbol{x}} \in \Omega_m, \tag{2e}$$

$$\tilde{C}(\tilde{\boldsymbol{x}}, 0) = \tilde{c}_{\text{init}}(\tilde{\boldsymbol{x}}) \quad \text{for } \tilde{\boldsymbol{x}} \in \Omega_b, \tag{2f}$$

where $\boldsymbol{n}$ is the unit normal of the bacterial membrane pointing into the surrounding medium. The function $\tilde{c}_{\text{init}}(\tilde{\boldsymbol{x}})$ appearing in the initial conditions (2e) and (2f) is continuous across the bacterial membrane and allows for a slow variation of the nutrient concentration in space. To close the system (2), we also require boundary conditions at the external boundary of Ω. However, to keep the generality of our analysis we will not impose a specific form in this paper.

In general, the typical diameter of bacterial *cocci* is around $2\tilde{R} \approx 1\,\mu$m, and a fermentation process would start with a cell density of around 10^8 cells/ml and end with a cell density of around 10^{11} cells/ml, corresponding to the approximate cell spacing $\epsilon l \approx 2 - 20\,\mu$m [21, 22]. Additionally, cell growth occurs on a much slower timescale than nutrient transport. It is generally possible to obtain the diffusion coefficient of a given nutrient within water and, for example, the diffusivities of dissolved carbon dioxide, nitrogen, and oxygen within water at room temperature are each around $2\,\text{cm}^2/\text{s}$ (with a maximum variation away from this value of 6%). However, it is much trickier to get pointwise diffusion and uptake coefficients within bacteria due to the difficulties in isolating and imaging a single bacterium. Partly for this reason, and also for a more general analysis (protozoa, for example, can have diameters $> 100\,\mu$m), it will be instructive to consider the various distinguished asymptotic limits of this problem.

2.1. Dimensionless equations. We scale the variables via $\tilde{\boldsymbol{x}} = l\boldsymbol{x}$, $\tilde{t} = (l^2/D_m)t$, $\tilde{R} = \epsilon l R$, $(\tilde{c}, \tilde{C}, \tilde{c}_{\text{init}}) = c_\infty(c, C, c_{\text{init}})$, where c_∞ is a characteristic concentration scale, to yield the dimensionless equations

$$\frac{\partial c}{\partial t} = \nabla^2 c \quad \text{for } \boldsymbol{x} \in \Omega_m, \tag{3a}$$

$$\frac{\partial C}{\partial t} = D\left(\nabla^2 C - \mu C\right) \quad \text{for } \boldsymbol{x} \in \Omega_b, \tag{3b}$$

$$c = C \quad \text{for } \boldsymbol{x} \in \partial\Omega_b, \tag{3c}$$

$$\boldsymbol{n} \cdot \nabla c = \boldsymbol{n} \cdot D\nabla C \quad \text{for } \boldsymbol{x} \in \partial\Omega_b, \tag{3d}$$

$$c(\boldsymbol{x}, 0) = c_{\text{init}}(\boldsymbol{x}) \quad \text{for } \boldsymbol{x} \in \Omega_m, \tag{3e}$$

$$C(\boldsymbol{x}, 0) = c_{\text{init}}(\boldsymbol{x}) \quad \text{for } \boldsymbol{x} \in \Omega_b, \tag{3f}$$

where $D = D_b/D_m$ is the ratio of diffusion coefficient in the medium to that in the bacteria, and $\mu = \lambda l^2/D_b$ is the ratio of the timescales of diffusion within the bacteria to uptake. The inclusion of the dimensionless diffusivity D in the definition of the dimensionless uptake rate $D\mu$ is for subsequent convenience. We do not specify the asymptotic orders of these dimensionless parameters yet, but later we consider the

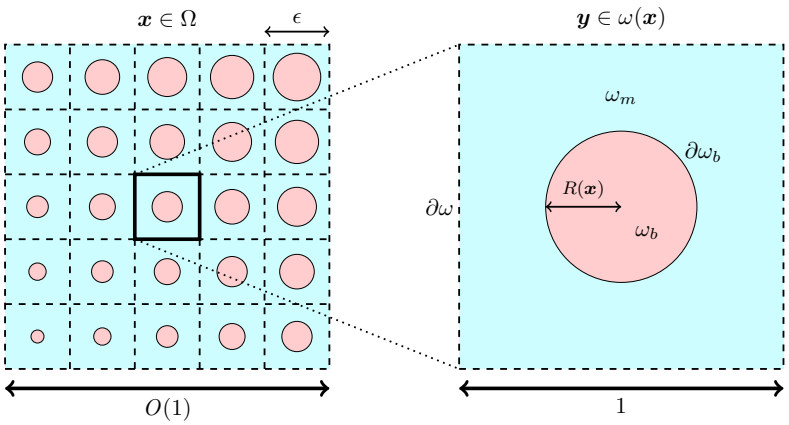

FIG. 1. *A two-dimensional projection of the three-dimensional problem we consider. The full problem is shown in the left figure, from which the cell problem (with* $\boldsymbol{y} \in [-1/2, 1/2]^3$*) is magnified and shown in the right figure. The nutrient diffuses with different diffusion coefficients in the blue passive medium and in the pink bacteria and is absorbed within the bacteria at a rate proportional to its concentration. We couple the regions via continuity of concentration and concentration flux. (Color available online.)*

three asymptotic limits over the timescale of macroscale diffusion in the medium, where $t = O(1)$.

In dimensionless units, the bacteria now form a cubic lattice of spheres whose centers are a distance of ϵ apart, and a bacterium centered at $\boldsymbol{x}$ has radius $\epsilon R(\boldsymbol{x})$. A schematic of this set-up is shown in Figure 1.

3. Deriving effective equations. Our goal is to upscale the governing equations (3) using a homogenization procedure via the method of multiple scales. Essentially, we introduce the additional spatial variable

$$\boldsymbol{y} = \frac{\boldsymbol{x} - \lfloor \boldsymbol{x} \rfloor}{\epsilon} - \boldsymbol{b}, \tag{4}$$

where we treat $\boldsymbol{x}$ and $\boldsymbol{y}$ as independent. In (4), we introduce the constant translation vector $\boldsymbol{b} = (1/2, 1/2, 1/2)$ for notational purposes. Thus, the microscale variable $\boldsymbol{y} \in [-1/2, 1/2]^3$ is defined within a unit cell $\omega(\boldsymbol{x})$, centered around one bacterium, and our dependent variables are now $c(\boldsymbol{x}, \boldsymbol{y}, t)$ and $C(\boldsymbol{x}, \boldsymbol{y}, t)$. The extra freedom that arises from introducing $\boldsymbol{y}$ is later removed by imposing that the problem is 1-periodic in each component of $\boldsymbol{y}$. Within each cell, we define several regions for convenience. The bacterium and medium phases are defined as $\omega_b(\boldsymbol{x})$ and $\omega_m(\boldsymbol{x})$, respectively. The spherical bacterial membrane between these two phases is defined as $\partial\omega_b(\boldsymbol{x})$. Finally, the cubic outer boundary of the cell is defined as $\partial\omega$. Formally, these sets are defined as

$$\omega_b = \{\boldsymbol{y} \in [-1/2, 1/2]^3 : \|\boldsymbol{y}\| < R(\boldsymbol{x})\}, \tag{5a}$$

$$\omega_m = \{\boldsymbol{y} \in [-1/2, 1/2]^3 : \|\boldsymbol{y}\| > R(\boldsymbol{x})\}, \tag{5b}$$

$$\partial\omega_b = \{\boldsymbol{y} \in [-1/2, 1/2]^3 : \|\boldsymbol{y}\| = R(\boldsymbol{x})\}, \tag{5c}$$

$$\partial\omega = \{\boldsymbol{y} \in [-1/2, 1/2]^3 : \|\boldsymbol{y}\|_\infty = 1/2\}, \tag{5d}$$

where $\|\cdot\|$ and $\|\cdot\|_\infty$ are the three-dimensional Euclidean and infinity norms, respectively.

We are interested in deriving effective governing equations for two quantities. First, $\widehat{c}(\boldsymbol{x},t)$, the intrinsic-averaged concentration within the medium, is defined as

$$\widehat{c}(\boldsymbol{x},t) = \frac{1}{|\omega_m(\boldsymbol{x})|}\int_{\omega_m(\boldsymbol{x})} c(\boldsymbol{x},\boldsymbol{y},t)\,\mathrm{d}\boldsymbol{y}, \tag{6a}$$

where $|\cdot|$ is the volume. The intrinsic-averaged concentration is important because it is the experimentally measurable concentration. Second, $\bar{c}(\boldsymbol{x},t)$, the volumetric-averaged concentration, is defined as

$$\begin{aligned}\bar{c}(\boldsymbol{x},t) &= \frac{1}{|\omega(\boldsymbol{x})|}\left(\int_{\omega_m(\boldsymbol{x})} c(\boldsymbol{x},\boldsymbol{y},t)\,\mathrm{d}\boldsymbol{y} + \int_{\omega_b(\boldsymbol{x})} C(\boldsymbol{x},\boldsymbol{y},t)\,\mathrm{d}\boldsymbol{y}\right)\\ &= \int_{\omega_m(\boldsymbol{x})} c(\boldsymbol{x},\boldsymbol{y},t)\,\mathrm{d}\boldsymbol{y} + \int_{\omega_b(\boldsymbol{x})} C(\boldsymbol{x},\boldsymbol{y},t)\,\mathrm{d}\boldsymbol{y}.\end{aligned} \tag{6b}$$

The volumetric-averaged concentration is a fundamental physical quantity of interest, as it can be used to determine the total number of moles of nutrient in the system.

Treating each dependent variable as a function of both $\boldsymbol{x}$ and $\boldsymbol{y}$, the spatial derivatives transform as follows:

$$\nabla \mapsto \nabla_{\boldsymbol{x}} + \frac{1}{\epsilon}\nabla_{\boldsymbol{y}}, \tag{7}$$

where $\nabla_{\boldsymbol{x}}$ and $\nabla_{\boldsymbol{y}}$ refer to the nabla operator in the $\boldsymbol{x}$- and $\boldsymbol{y}$-coordinate systems, respectively. The spatial transformation (7) also causes the unit normal on the boundary to transform (as also occurs in, for example, [30, 5]). This can be seen by defining the function $\chi(\boldsymbol{x},\boldsymbol{y}) = \|\boldsymbol{y}\| - R(\boldsymbol{x})$, noting that the bacterial membrane is defined by $\chi = 0$ and thus $\boldsymbol{n} = \nabla\chi/\|\nabla\chi\|$, and then using (7) to yield

$$\boldsymbol{n} \mapsto \frac{\boldsymbol{n}_{\boldsymbol{y}} - \epsilon\nabla_{\boldsymbol{x}}R}{\|\boldsymbol{n}_{\boldsymbol{y}} - \epsilon\nabla_{\boldsymbol{x}}R\|}, \tag{8}$$

where $\boldsymbol{n}_{\boldsymbol{y}} = \boldsymbol{y}/\|\boldsymbol{y}\|$. This transformation of the boundary is sometimes referred to as the level-set framework, as discussed in section 1.

Using the transformations (7) and (8), the dimensionless governing equations (3) become

$$\epsilon^2\frac{\partial c}{\partial t} = (\nabla_{\boldsymbol{y}} + \epsilon\nabla_{\boldsymbol{x}})\cdot(\nabla_{\boldsymbol{y}} + \epsilon\nabla_{\boldsymbol{x}})\,c \quad \text{for } \boldsymbol{y}\in\omega_m(\boldsymbol{x}), \tag{9a}$$

$$\epsilon^2\frac{\partial C}{\partial t} = D\,(\nabla_{\boldsymbol{y}} + \epsilon\nabla_{\boldsymbol{x}})\cdot(\nabla_{\boldsymbol{y}} + \epsilon\nabla_{\boldsymbol{x}})\,C - \epsilon^2 D\mu C \quad \text{for } \boldsymbol{y}\in\omega_b(\boldsymbol{x}), \tag{9b}$$

$$c = C \quad \text{for } \boldsymbol{y}\in\partial\omega_b(\boldsymbol{x}), \tag{9c}$$

$$(\boldsymbol{n}_{\boldsymbol{y}} - \epsilon\nabla_{\boldsymbol{x}}R)\cdot(\nabla_{\boldsymbol{y}} + \epsilon\nabla_{\boldsymbol{x}})\,c = (\boldsymbol{n}_{\boldsymbol{y}} - \epsilon\nabla_{\boldsymbol{x}}R)\cdot D\,(\nabla_{\boldsymbol{y}} + \epsilon\nabla_{\boldsymbol{x}})\,C \quad \text{for } \boldsymbol{y}\in\partial\omega_b(\boldsymbol{x}), \tag{9d}$$

$$c(\boldsymbol{x},\boldsymbol{y},0) = c_{\mathrm{init}}(\boldsymbol{x}) \quad \text{for } \boldsymbol{y}\in\omega_m(\boldsymbol{x}), \tag{9e}$$

$$C(\boldsymbol{x},\boldsymbol{y},0) = c_{\mathrm{init}}(\boldsymbol{x}) \quad \text{for } \boldsymbol{y}\in\omega_b(\boldsymbol{x}), \tag{9f}$$

$$c \text{ periodic} \quad \text{for } \boldsymbol{y}\in\partial\omega, \tag{9g}$$

where (9g) is imposed to remove secular terms in the method of multiple scales. Here and hereafter, any condition similar to (9g) refers only to periodicity in the dependent variable $\boldsymbol{y}$.

TABLE 1

A summary of the three distinguished asymptotic limits we consider in this paper. Note that R has already been scaled by ϵ so that, when $O(1)$, it is of the same asymptotic order as the periodic-cell size.

	D	μ	R
Case 1	$O(1)$	$O(1)$	$O(1)$
Case 2	$O(\epsilon^2)$	$O(1/\epsilon^2)$	$O(1)$
Case 3	$O(1)$	$O(1/\epsilon^6)$	$O(\epsilon^2)$

We are interested in the physical scenarios in which the effective uptake balances the macroscale diffusion over the timescale of the latter, which occurs over $t = O(1)$. There are three distinguished asymptotic limits: (i) standard diffusion, uptake, and obstacle size; (ii) small diffusion, large uptake, and standard obstacle size; (iii) standard diffusion, very large uptake, and small obstacle size. We summarize the three asymptotic limits in Table 1. We note that, in the absence of any source or sink terms from the external boundary, the removal rate of nutrient in the system can be deduced from (3) as follows:

$$\frac{\partial}{\partial t}\left(\int_{\Omega_m} c\,\mathrm{d}\boldsymbol{x} + \int_{\Omega_b} C\,\mathrm{d}\boldsymbol{x}\right) = -\mu D \int_{\Omega_b} C\,\mathrm{d}\boldsymbol{x}. \tag{10}$$

When uptake within a bacterium occurs over the entire bacterium domain and not just within a boundary layer near the bacterial membrane, we see from (10) that an $O(1)$ uptake timescale (corresponding to diffusion over the timescale of macroscale diffusion) occurs when $\mu D R^3 = O(1)$. This constraint helps to elucidate the relative scalings within each case in Table 1. We proceed by homogenizing the system in each of the three cases mentioned above.

3.1. Case 1: Standard diffusion, uptake, and bacterial size: $D = O(1)$, $\mu = O(1)$, $R = O(1)$. The first distinguished limit we consider is $D = O(1)$, $\mu = O(1)$, and $R = O(1)$. While this limit is only a specific example of the general classical case (section 5.3 in [16]) with a discontinuous diffusion coefficient, it does provide the distinguished limit for the effective diffusion for the remaining cases, and so we include it for completeness. To upscale the system, we introduce the asymptotic expansions

$$c = c_0(\boldsymbol{x},\boldsymbol{y},t) + \epsilon c_1(\boldsymbol{x},\boldsymbol{y},t) + \epsilon^2 c_2(\boldsymbol{x},\boldsymbol{y},t) + O(\epsilon^3), \tag{11a}$$

$$C = C_0(\boldsymbol{x},\boldsymbol{y},t) + \epsilon C_1(\boldsymbol{x},\boldsymbol{y},t) + \epsilon^2 C_2(\boldsymbol{x},\boldsymbol{y},t) + O(\epsilon^3), \tag{11b}$$

substitute these into (9), and equate terms of equal magnitude.

The leading-order terms in (9) are

$$0 = \nabla_{\boldsymbol{y}}^2 c_0 \quad \text{for } \boldsymbol{y} \in \omega_m(\boldsymbol{x}), \tag{12a}$$

$$0 = D\nabla_{\boldsymbol{y}}^2 C_0 \quad \text{for } \boldsymbol{y} \in \omega_b(\boldsymbol{x}), \tag{12b}$$

$$c_0 = C_0 \quad \text{for } \boldsymbol{y} \in \partial\omega_b(\boldsymbol{x}), \tag{12c}$$

$$\boldsymbol{n}_{\boldsymbol{y}} \cdot \nabla_{\boldsymbol{y}} c_0 = D\boldsymbol{n}_{\boldsymbol{y}} \cdot \nabla_{\boldsymbol{y}} C_0 \quad \text{for } \boldsymbol{y} \in \partial\omega_b(\boldsymbol{x}), \tag{12d}$$

$$c_0(\boldsymbol{x},\boldsymbol{y},0) = c_{\mathrm{init}}(\boldsymbol{x}) \quad \text{for } \boldsymbol{y} \in \omega_m(\boldsymbol{x}), \tag{12e}$$

$$C_0(\boldsymbol{x},\boldsymbol{y},0) = c_{\mathrm{init}}(\boldsymbol{x}) \quad \text{for } \boldsymbol{y} \in \omega_b(\boldsymbol{x}), \tag{12f}$$

$$c_0 \text{ periodic} \quad \text{for } \boldsymbol{y} \in \partial\omega. \tag{12g}$$

The system (12) yields solutions that are independent of $\boldsymbol{y}$, and thus $c_0 = c_0(\boldsymbol{x}, t)$ and $C_0 = C_0(\boldsymbol{x}, t)$, with $c_0 = C_0$ and $c_0(\boldsymbol{x}, 0) = C_0(\boldsymbol{x}, 0) = c_{\text{init}}(\boldsymbol{x})$. To close the problem at leading order, we must derive a solvability condition from higher asymptotic orders.

The relevant $O(\epsilon)$ terms in (9) yield

$$0 = \nabla_{\boldsymbol{y}}^2 c_1 \quad \text{for } \boldsymbol{y} \in \omega_m(\boldsymbol{x}), \tag{13a}$$

$$0 = D\nabla_{\boldsymbol{y}}^2 C_1 \quad \text{for } \boldsymbol{y} \in \omega_b(\boldsymbol{x}), \tag{13b}$$

$$c_1 = C_1 \quad \text{for } \boldsymbol{y} \in \partial\omega_b(\boldsymbol{x}), \tag{13c}$$

$$\boldsymbol{n}_{\boldsymbol{y}} \cdot (\nabla_{\boldsymbol{y}} c_1 + \nabla_{\boldsymbol{x}} c_0) = D\boldsymbol{n}_{\boldsymbol{y}} \cdot (\nabla_{\boldsymbol{y}} C_1 + \nabla_{\boldsymbol{x}} C_0) \quad \text{for } \boldsymbol{y} \in \partial\omega_b(\boldsymbol{x}), \tag{13d}$$

$$c_1 \text{ periodic} \quad \text{for } \boldsymbol{y} \in \partial\omega. \tag{13e}$$

We may express the solutions to (13) in the form

$$c_1(\boldsymbol{x}, \boldsymbol{y}, t) = -\boldsymbol{\xi}(\boldsymbol{x}, \boldsymbol{y}) \cdot \nabla_{\boldsymbol{x}} c_0(\boldsymbol{x}, t) + \breve{c}_1(\boldsymbol{x}, t), \tag{14a}$$

$$C_1(\boldsymbol{x}, \boldsymbol{y}, t) = -\boldsymbol{\Xi}(\boldsymbol{x}, \boldsymbol{y}) \cdot \nabla_{\boldsymbol{x}} C_0(\boldsymbol{x}, t) + \breve{C}_1(\boldsymbol{x}, t), \tag{14b}$$

where $\breve{c}_1$ and $\breve{C}_1$ are (thus far) arbitrary functions of $\boldsymbol{x}$ and t only, which we shall not need to calculate to obtain the leading-order homogenized problem. The components ξ_i and Ξ_i of the zero-mean (over a single cell) functions $\boldsymbol{\xi}$ and $\boldsymbol{\Xi}$ satisfy the cell problems

$$0 = \nabla_{\boldsymbol{y}}^2 \xi_i \quad \text{for } \boldsymbol{y} \in \omega_m(\boldsymbol{x}), \tag{15a}$$

$$0 = D\nabla_{\boldsymbol{y}}^2 \Xi_i \quad \text{for } \boldsymbol{y} \in \omega_b(\boldsymbol{x}), \tag{15b}$$

$$\xi_i = \Xi_i \quad \text{for } \boldsymbol{y} \in \partial\omega_b(\boldsymbol{x}), \tag{15c}$$

$$\boldsymbol{n}_{\boldsymbol{y}} \cdot (\nabla_{\boldsymbol{y}} \xi_i - D\nabla_{\boldsymbol{y}} \Xi_i) = (1 - D)\, \boldsymbol{n}_{\boldsymbol{y}} \cdot \boldsymbol{e}_i \quad \text{for } \boldsymbol{y} \in \partial\omega_b(\boldsymbol{x}), \tag{15d}$$

$$\xi_i \text{ periodic} \quad \text{for } \boldsymbol{y} \in \partial\omega, \tag{15e}$$

where $\boldsymbol{e}_i$ is the unit vector in the y_i-direction.

Finally, from the relevant $O(\epsilon^2)$ terms in (9), we obtain

$$\frac{\partial c_0}{\partial t} = \nabla_{\boldsymbol{y}} \cdot (\nabla_{\boldsymbol{y}} c_2 + \nabla_{\boldsymbol{x}} c_1) + \nabla_{\boldsymbol{x}} \cdot (\nabla_{\boldsymbol{y}} c_1 + \nabla_{\boldsymbol{x}} c_0) \quad \text{for } \boldsymbol{y} \in \omega_m(\boldsymbol{x}), \tag{16a}$$

$$\frac{\partial C_0}{\partial t} = D\nabla_{\boldsymbol{y}} \cdot (\nabla_{\boldsymbol{y}} C_2 + \nabla_{\boldsymbol{x}} C_1) + D\nabla_{\boldsymbol{x}} \cdot (\nabla_{\boldsymbol{y}} C_1 + \nabla_{\boldsymbol{x}} C_0) - D\mu C_0 \quad \text{for } \boldsymbol{y} \in \omega_b(\boldsymbol{x}), \tag{16b}$$

$$c_2 = C_2 \quad \text{for } \boldsymbol{y} \in \partial\omega_b(\boldsymbol{x}), \tag{16c}$$

$$\begin{aligned} \boldsymbol{n}_{\boldsymbol{y}} \cdot (\nabla_{\boldsymbol{y}} c_2 + \nabla_{\boldsymbol{x}} c_1) - \nabla_{\boldsymbol{x}} R \cdot (\nabla_{\boldsymbol{y}} c_1 + \nabla_{\boldsymbol{x}} c_0) \\ = D\left(\boldsymbol{n}_{\boldsymbol{y}} \cdot (\nabla_{\boldsymbol{y}} C_2 + \nabla_{\boldsymbol{x}} C_1) - \nabla_{\boldsymbol{x}} R \cdot (\nabla_{\boldsymbol{y}} C_1 + \nabla_{\boldsymbol{x}} C_0)\right) \quad \text{for } \boldsymbol{y} \in \partial\omega_b(\boldsymbol{x}), \end{aligned} \tag{16d}$$

$$c_2 \text{ periodic} \quad \text{for } \boldsymbol{y} \in \partial\omega. \tag{16e}$$

To derive effective equations for the averaged concentrations defined in (6), we integrate (16a) over the domain $\omega_m(\boldsymbol{x})$ and (16b) over the domain $\omega_b(\boldsymbol{x})$, sum the results, and then apply the divergence theorem with the boundary conditions (16d,e) to obtain

$$\begin{aligned} \int_{\omega_m(\boldsymbol{x})} \frac{\partial c_0}{\partial t}\, \mathrm{d}\boldsymbol{y} + \int_{\omega_b(\boldsymbol{x})} \frac{\partial C_0}{\partial t}\, \mathrm{d}\boldsymbol{y} = \int_{\omega_m(\boldsymbol{x})} \nabla_{\boldsymbol{x}} \cdot (\nabla_{\boldsymbol{y}} c_1 + \nabla_{\boldsymbol{x}} c_0)\, \mathrm{d}\boldsymbol{y} \\ - \int_{\partial\omega_b(\boldsymbol{x})} \nabla_{\boldsymbol{x}} R \cdot (\nabla_{\boldsymbol{y}} c_1 + \nabla_{\boldsymbol{x}} c_0)\, \mathrm{d}s + D \int_{\omega_b(\boldsymbol{x})} \nabla_{\boldsymbol{x}} \cdot (\nabla_{\boldsymbol{y}} C_1 + \nabla_{\boldsymbol{x}} C_0)\, \mathrm{d}\boldsymbol{y} \end{aligned}$$

$$-D\int_{\partial\omega_b(\boldsymbol{x})}\nabla_{\boldsymbol{x}}R\cdot(\nabla_{\boldsymbol{y}}C_1+\nabla_{\boldsymbol{x}}C_0)\,\mathrm{d}s-D\mu\int_{\omega_b(\boldsymbol{x})}C_0\,\mathrm{d}\boldsymbol{y}, \tag{17}$$

where $\mathrm{d}s$ is the surface element of the bacterial membrane $\partial\omega_b(\boldsymbol{x})$. Using the Reynolds transport theorem to combine the first and second integrals on the right-hand side of (17) as well as the third and fourth integrals, we obtain

$$\begin{aligned}|\omega_m(\boldsymbol{x})|\frac{\partial c_0}{\partial t}+|\omega_b(\boldsymbol{x})|\frac{\partial C_0}{\partial t}&=\nabla_{\boldsymbol{x}}\cdot\int_{\omega_m(\boldsymbol{x})}(\nabla_{\boldsymbol{y}}c_1+\nabla_{\boldsymbol{x}}c_0)\,\mathrm{d}\boldsymbol{y}\\ &+D\nabla_{\boldsymbol{x}}\cdot\int_{\omega_b(\boldsymbol{x})}(\nabla_{\boldsymbol{y}}C_1+\nabla_{\boldsymbol{x}}C_0)\,\mathrm{d}\boldsymbol{y}-D\mu|\omega_b(\boldsymbol{x})|C_0\end{aligned} \tag{18}$$

as the solvability condition required to close the leading-order problem. We note that $|\omega_m|+|\omega_b|=1$, and that $|\omega_b|=4\pi R^3/3$ for the spherical bacteria we consider in this paper.

We can use (14) to deduce that $\nabla_{\boldsymbol{y}}c_1=-(\mathbf{J}_{\boldsymbol{\xi}}^{\mathrm{T}})\nabla_{\boldsymbol{x}}c_0$ and $\nabla_{\boldsymbol{y}}C_1=-(\mathbf{J}_{\boldsymbol{\Xi}}^{\mathrm{T}})\nabla_{\boldsymbol{x}}C_0$, where $(\mathbf{J}_{\boldsymbol{\xi}}^{\mathrm{T}})_{ij}=\partial\xi_j/\partial y_i$ and $(\mathbf{J}_{\boldsymbol{\Xi}}^{\mathrm{T}})_{ij}=\partial\Xi_j/\partial y_i$ are the transposes of the Jacobian matrices of $\boldsymbol{\xi}$ and $\boldsymbol{\Xi}$, respectively, these being the vector solutions to the cell problems defined in (15). Using these results, recalling that $c_0=C_0$ from the leading-order equations, and noting that the leading-order independence of c_0 on $\boldsymbol{y}$ leads to the asymptotic result $\widehat{c}\sim c_0$ in (6a), we rewrite (18) as

$$\frac{\partial\widehat{c}}{\partial t}=\nabla_{\boldsymbol{x}}\cdot\left(\widehat{D}(\boldsymbol{x})\nabla_{\boldsymbol{x}}\widehat{c}\right)-\frac{4}{3}\pi D\mu R^3\widehat{c}, \tag{19a}$$

at leading order, with the initial condition

$$\widehat{c}(\boldsymbol{x},0)=c_{\mathrm{init}}(\boldsymbol{x}), \tag{19b}$$

obtained by substituting (12e) into (6a). The homogenized diffusion tensor is defined as

$$\widehat{D}(\boldsymbol{x})\mathbf{I}=\int_{\omega_m(\boldsymbol{x})}\left(\mathbf{I}-\mathbf{J}_{\boldsymbol{\xi}}^{\mathrm{T}}\right)\,\mathrm{d}\boldsymbol{y}+D\int_{\omega_b(\boldsymbol{x})}\left(\mathbf{I}-\mathbf{J}_{\boldsymbol{\Xi}}^{\mathrm{T}}\right)\,\mathrm{d}\boldsymbol{y}, \tag{19c}$$

and $\mathbf{I}$ is the three-dimensional identity matrix. In the case of spherical bacteria, the homogenized diffusion tensor is a multiple of the identity matrix due to the symmetry of the cell problem (15). That is,

$$\int_{\omega_m(\boldsymbol{x})}\mathbf{J}_{\boldsymbol{\xi}}^{\mathrm{T}}\,\mathrm{d}\boldsymbol{y}=\left(\int_{\omega_m(\boldsymbol{x})}\partial\xi_i/\partial y_i\,\mathrm{d}\boldsymbol{y}\right)\mathbf{I},\qquad\int_{\omega_b(\boldsymbol{x})}\mathbf{J}_{\boldsymbol{\Xi}}^{\mathrm{T}}\,\mathrm{d}\boldsymbol{y}=\left(\int_{\omega_b(\boldsymbol{x})}\partial\Xi_j/\partial y_j\,\mathrm{d}\boldsymbol{y}\right)\mathbf{I} \tag{20}$$

for $i,j=1,2,3$, with ξ_i and Ξ_j determined by (15). We are able to obtain analytic bounds on the effective diffusion coefficient using the Voigt–Reiss inequality (equation (1.63) in [19]), yielding

$$\frac{D}{|\omega_b|+D|\omega_m|}\leqslant\widehat{D}\leqslant|\omega_m|+D|\omega_b|, \tag{21}$$

where we have used $|\omega|=1$.

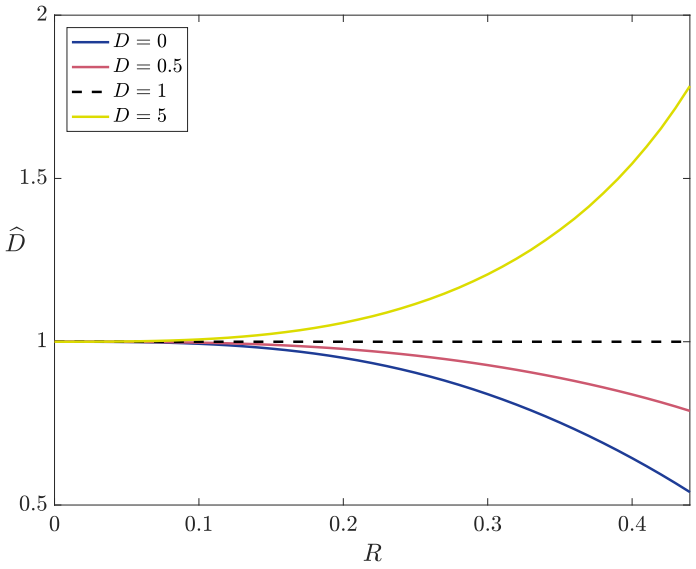

FIG. 2. *The effective diffusion coefficient derived in Case* 1*, which is the distinguished asymptotic limit for the diffusion coefficient in the other cases we consider. The effective diffusion coefficient in Case* 2 *is given by the limit* $D \to 0^+$*, and the effective diffusion coefficient in Case* 3 *is given by the limit* $R \to 0^+$*. That is, in Case* 3 *the effective dimensionless diffusion coefficient is unity.*

We note that $\widehat{D}$ is a function of two parameters in this problem: the diffusion ratio D and the bacterium radius R. We solve the cell problem (15) using the software package COMSOL Multiphysics to determine the effective diffusion coefficients, leading to the results in Figure 2. As physically expected, when diffusion is slower within the bacteria than in the passive medium, the effective diffusion is slower than the pointwise diffusion in the passive medium, and vice versa for a quicker diffusion within the bacteria. Moreover, this effect is greater when the bacterial volume is larger. We note that when $D = 1$, the solutions to the cell problem (15) are independent of $\boldsymbol{y}$, resulting in $\widehat{D} \equiv 1$.

For our main goal of analyzing the effective uptake, we see from (19a) that, in Case 1, the effective uptake is equal to the product of the pointwise uptake and the bacterial volume. For our additional aim of obtaining an equation for the averaged concentration $\bar{c}(\boldsymbol{x}, t)$, we note that the leading-order behavior of (6b) is given by

$$\bar{c}(\boldsymbol{x}, t) \sim \widehat{c}(\boldsymbol{x}, t). \tag{22}$$

Thus, from (19) we deduce that the effective governing equation for $\bar{c}$ is

$$\frac{\partial \bar{c}}{\partial t} = \nabla_{\boldsymbol{x}} \cdot \left(\widehat{D}(\boldsymbol{x}) \nabla_{\boldsymbol{x}} \bar{c} \right) - \frac{4}{3} \pi D \mu R^3 \bar{c}, \tag{23a}$$

with initial condition

$$\bar{c}(\boldsymbol{x}, 0) = c_{\text{init}}(\boldsymbol{x}), \tag{23b}$$

obtained by substituting (12e) and (12f) into (6b). The generalization of this result to arbitrary bacterial shapes is briefly discussed in Appendix A.

The effective governing equation (19) holds for $O(1)$ values of μ and D. However, when μ is large and D is small, with $\mu D = O(1)$, the effective equation (19) is not correct over an $O(1)$ timescale. We may anticipate the significant change in behavior in this limit from the terms in (9) switching asymptotic orders, and we explore this limit in the next section.

3.2. Case 2: Small diffusion within the bacteria: $D = O(\epsilon^2)$, $\mu = O(1/\epsilon^2)$, $R = O(1)$. The second distinguished limit we consider is $D = O(\epsilon^2)$, $\mu = O(1/\epsilon^2)$, and $R = O(1)$. We consider this limit by setting $D = \epsilon^2 \hat{D}$ and $\mu = \hat{\mu}/\epsilon^2$, where $\hat{D}$ and $\hat{\mu}$ are both of $O(1)$. As there is a large difference between the diffusion coefficients in the medium and bacterium, this is a double-porosity model. As discussed in section 1, such models tend to induce a memory effect in the upscaled effective equations, whereby the history of the system is required to determine the current state of the system. We will find a similar effect in this case—the partial differential equations being upscaled into integrodifferential equations.

We introduce the asymptotic expansions

$$c = c_0(\boldsymbol{x}, \boldsymbol{y}, t) + \epsilon c_1(\boldsymbol{x}, \boldsymbol{y}, t) + \epsilon^2 c_2(\boldsymbol{x}, \boldsymbol{y}, t) + O(\epsilon^3), \quad C = C_0(\boldsymbol{x}, \boldsymbol{y}, t) + O(\epsilon) \tag{24}$$

to the governing equations (9), noting that we will only require the leading-order term in C for the following analysis. The leading-order terms in (9) are

$$0 = \nabla_{\boldsymbol{y}}^2 c_0 \quad \text{for } \boldsymbol{y} \in \omega_m(\boldsymbol{x}), \tag{25a}$$

$$\frac{\partial C_0}{\partial t} = \hat{D}\left(\nabla_{\boldsymbol{y}}^2 C_0 - \hat{\mu} C_0\right) \quad \text{for } \boldsymbol{y} \in \omega_b(\boldsymbol{x}), \tag{25b}$$

$$c_0 = C_0 \quad \text{for } \boldsymbol{y} \in \partial\omega_b(\boldsymbol{x}), \tag{25c}$$

$$\boldsymbol{n}_{\boldsymbol{y}} \cdot \nabla_{\boldsymbol{y}} c_0 = 0 \quad \text{for } \boldsymbol{y} \in \partial\omega_b(\boldsymbol{x}), \tag{25d}$$

$$c_0(\boldsymbol{x}, \boldsymbol{y}, 0) = c_{\text{init}}(\boldsymbol{x}) \quad \text{for } \boldsymbol{y} \in \omega_m(\boldsymbol{x}), \tag{25e}$$

$$C_0(\boldsymbol{x}, \boldsymbol{y}, 0) = c_{\text{init}}(\boldsymbol{x}) \quad \text{for } \boldsymbol{y} \in \omega_b(\boldsymbol{x}), \tag{25f}$$

$$c_0 \text{ periodic} \quad \text{for } \boldsymbol{y} \in \partial\omega. \tag{25g}$$

The system for c_0 is defined by (25a,d,e,g) and decouples from C_0. We see that c_0 is independent of $\boldsymbol{y}$, and thus $c_0 = c_0(\boldsymbol{x}, t)$ with $c_0(\boldsymbol{x}, 0) = c_{\text{init}}(\boldsymbol{x})$. We solve for C_0 later in this section.

The important $O(\epsilon)$ problem is for c_1, for which we obtain the following system:

$$0 = \nabla_{\boldsymbol{y}}^2 c_1 \quad \text{for } \boldsymbol{y} \in \omega_m(\boldsymbol{x}), \tag{26a}$$

$$\boldsymbol{n}_{\boldsymbol{y}} \cdot \nabla_{\boldsymbol{y}} c_1 = -\boldsymbol{n}_{\boldsymbol{y}} \cdot \nabla_{\boldsymbol{x}} c_0 \quad \text{for } \boldsymbol{y} \in \partial\omega_b(\boldsymbol{x}), \tag{26b}$$

$$c_1 \text{ periodic} \quad \text{for } \boldsymbol{y} \in \partial\omega. \tag{26c}$$

The system (26) is equivalent to taking the limit of $D \to 0$ in (13). Moreover, it is the same first-correction problem that arises in [5, 11]. In a similar manner to the analysis in section 3.1, we may solve (26) by setting

$$c_1(\boldsymbol{x}, \boldsymbol{y}, t) = -\boldsymbol{\gamma}(\boldsymbol{x}, \boldsymbol{y}) \cdot \nabla_{\boldsymbol{x}} c_0(\boldsymbol{x}, t) + \check{c}(\boldsymbol{x}, t), \tag{27}$$

where $\check{c}$ is an arbitrary function of $\boldsymbol{x}$ and t only, and the components γ_i of the zero-mean (over a single cell) function $\boldsymbol{\gamma}$ satisfy the cell problem

$$0 = \nabla_{\boldsymbol{y}}^2 \gamma_i \quad \text{for } \boldsymbol{y} \in \omega_m(\boldsymbol{x}), \tag{28a}$$

$$\boldsymbol{n_y} \cdot \nabla_{\boldsymbol{y}} \gamma_i = \boldsymbol{n_y} \cdot \boldsymbol{e}_i \quad \text{for } \boldsymbol{y} \in \partial\omega_b(\boldsymbol{x}), \tag{28b}$$

$$\gamma_i \text{ periodic} \quad \text{for } \boldsymbol{y} \in \partial\omega, \tag{28c}$$

where $\boldsymbol{e}_i$ is the unit vector in the y_i-direction. The cell problem (28) for γ_i is equivalent to the system (15) for ξ_i in the limit of $D \to 0$.

The relevant $O(\epsilon^2)$ problem is

$$\frac{\partial c_0}{\partial t} = \nabla_{\boldsymbol{y}} \cdot (\nabla_{\boldsymbol{y}} c_2 + \nabla_{\boldsymbol{x}} c_1) + \nabla_{\boldsymbol{x}} \cdot (\nabla_{\boldsymbol{y}} c_1 + \nabla_{\boldsymbol{x}} c_0) \quad \text{for } \boldsymbol{y} \in \omega_m(\boldsymbol{x}), \tag{29a}$$

$$\boldsymbol{n_y} \cdot (\nabla_{\boldsymbol{y}} c_2 + \nabla_{\boldsymbol{x}} c_1) - \nabla_{\boldsymbol{x}} R \cdot (\nabla_{\boldsymbol{y}} c_1 + \nabla_{\boldsymbol{x}} c_0) = \boldsymbol{n_y} \cdot \hat{D} \nabla_{\boldsymbol{y}} C_0 \quad \text{for } \boldsymbol{y} \in \partial\omega_b(\boldsymbol{x}), \tag{29b}$$

$$c_2 \text{ periodic} \quad \text{for } \boldsymbol{y} \in \partial\omega. \tag{29c}$$

To derive effective equations for the averaged concentrations defined in (6), we proceed in a similar manner to section 3.1. We integrate (29a) over the domain $\omega_m(\boldsymbol{x})$, apply the divergence theorem, and use the boundary conditions (29b,c) to obtain

$$\begin{aligned}\int_{\omega_m(\boldsymbol{x})} \frac{\partial c_0}{\partial t} \,\mathrm{d}\boldsymbol{y} = \int_{\omega_m(\boldsymbol{x})} \nabla_{\boldsymbol{x}} \cdot (\nabla_{\boldsymbol{y}} c_1 + \nabla_{\boldsymbol{x}} c_0) \,\mathrm{d}\boldsymbol{y} - \int_{\partial\omega_b(\boldsymbol{x})} \nabla_{\boldsymbol{x}} R \cdot (\nabla_{\boldsymbol{y}} c_1 + \nabla_{\boldsymbol{x}} c_0) \,\mathrm{d}s \\ - \int_{\partial\omega_b(\boldsymbol{x})} \boldsymbol{n_y} \cdot \hat{D} \nabla_{\boldsymbol{y}} C_0 \,\mathrm{d}s.\end{aligned} \tag{30}$$

Using the Reynolds transport theorem to combine the first two integrals on the right-hand side of (30), we obtain

$$|\omega_m(\boldsymbol{x})| \frac{\partial c_0}{\partial t} = \nabla_{\boldsymbol{x}} \cdot \int_{\omega_m(\boldsymbol{x})} (\nabla_{\boldsymbol{y}} c_1 + \nabla_{\boldsymbol{x}} c_0) \,\mathrm{d}\boldsymbol{y} - \hat{D} |\partial\omega_b(\boldsymbol{x})| \left. \frac{\partial C_0}{\partial r} \right|_{r=R}. \tag{31}$$

We use (27) to determine that $\nabla_{\boldsymbol{y}} c_1 = -(\mathbf{J}_{\boldsymbol{\gamma}}^{\mathrm{T}}) \nabla_{\boldsymbol{x}} c_0$, where $(\mathbf{J}_{\boldsymbol{\gamma}}^{\mathrm{T}})_{ij} = \partial\gamma_j / \partial y_i$ is the transpose of the Jacobian matrix of $\boldsymbol{\gamma}$, the vector solution to the cell problems defined in (28). In the same manner as the previous case, we note that $\int_{\omega_m(\boldsymbol{x})} \mathbf{J}_{\boldsymbol{\gamma}}^{\mathrm{T}} \,\mathrm{d}\boldsymbol{y} = (\int_{\omega_m(\boldsymbol{x})} \partial\gamma_i / \partial y_i \,\mathrm{d}\boldsymbol{y}) \mathbf{I}$ for $i = 1, 2, 3$ with γ_i determined in (28), allowing us to write (31) as

$$|\omega_m(\boldsymbol{x})| \frac{\partial c_0}{\partial t} = \nabla_{\boldsymbol{x}} \cdot \left(|\omega_m| \overline{D}(\boldsymbol{x}) \nabla_{\boldsymbol{x}} c_0 \right) - \hat{D} |\partial\omega_b(\boldsymbol{x})| \left. \frac{\partial C_0}{\partial r} \right|_{r=R}, \tag{32}$$

where the classical homogenized diffusion tensor is defined as

$$\overline{D}(\boldsymbol{x}) \mathbf{I} = \left(\mathbf{I} - \frac{1}{|\omega_m|} \int_{\omega_m(\boldsymbol{x})} \mathbf{J}_{\boldsymbol{\gamma}}^{\mathrm{T}} \,\mathrm{d}\boldsymbol{y} \right). \tag{33}$$

The effective diffusion coefficient $\overline{D}$ we obtain here is identical to the effective diffusion coefficients derived in [5] and [11] for diffusion past impermeable spheres in a cubic array with no adsorption and surface adsorption, respectively (advection is also considered in [11]). This is because we have considered the small diffusivity limit within the bacteria, making the obstacles appear impermeable at leading order. We show this effective diffusion coefficient in Figure 2, as $\overline{D}$ is equivalent to $\widehat{D}$ when $D = 0$ in the latter. Thus, the effective diffusion coefficient in Case 2 is a sublimit of the effective diffusion coefficient in Case 1.

To obtain a governing equation for $\widehat{c}$ from (32), we first note that $\widehat{c} \sim c_0$ in (6a). This arises from the leading-order independence of c_0 on $\boldsymbol{y}$. Using (25b) and (25f), we can write (32) as

(34)
$$\frac{\partial}{\partial t}\left(|\omega_m(\boldsymbol{x})|\widehat{c} + \int_{\omega_b(\boldsymbol{x})} C_0(\boldsymbol{x},\boldsymbol{y},t)\,\mathrm{d}\boldsymbol{y}\right) = \nabla_{\boldsymbol{x}}\cdot\left(|\omega_m|\overline{D}(\boldsymbol{x})\nabla_{\boldsymbol{x}}\widehat{c}\right) - \hat{\mu}\hat{D}\int_{\omega_b(\boldsymbol{x})} C_0(\boldsymbol{x},\boldsymbol{y},t)\,\mathrm{d}\boldsymbol{y},$$

where C_0 depends on $\widehat{c}$ through the leading-order problem

$$\frac{\partial C_0}{\partial t} = \hat{D}\left(\nabla_{\boldsymbol{y}}^2 C_0 - \hat{\mu}C_0\right) \quad \text{for } \boldsymbol{y}\in\omega_b(\boldsymbol{x}), \tag{35a}$$

$$C_0 = \widehat{c}(\boldsymbol{x},t) \quad \text{for } \boldsymbol{y}\in\partial\omega_b(\boldsymbol{x}), \tag{35b}$$

$$C_0(\boldsymbol{x},\boldsymbol{y},0) = c_{\mathrm{init}}(\boldsymbol{x}) \quad \text{for } \boldsymbol{y}\in\omega_b(\boldsymbol{x}). \tag{35c}$$

We seek a radially symmetric solution for C_0 (in terms of $r = \|\boldsymbol{y}\|$), imposing $\partial C_0/\partial r = 0$ at $r = 0$ to ensure boundedness at the origin, and find a representation of the solution in the form

$$C_0(\boldsymbol{x},r,t) = \widehat{c}(\boldsymbol{x},t) + \frac{1}{r}\sum_{n=1}^{\infty} U_n(\boldsymbol{x},t)\sin a_n r, \tag{36a}$$

$$U_n(\boldsymbol{x},t) = e^{-\hat{D}(\hat{\mu}+a_n^2)t}\frac{2(-1)^n}{a_n}\int_0^t\left(\frac{\partial\widehat{c}}{\partial\tau} + \hat{\mu}\hat{D}\widehat{c}(\boldsymbol{x},\tau)\right)e^{\hat{D}(\hat{\mu}+a_n^2)\tau}\,\mathrm{d}\tau, \tag{36b}$$

$$a_n(\boldsymbol{x}) = \frac{n\pi}{R(\boldsymbol{x})}, \tag{36c}$$

where a_n represents the eigenvalues of the time-dependent problem. Integrating by parts the first term in the integrand of (36b) and rewriting the first term in (36a) in terms of a Fourier series in $\sin a_n r$ (essentially encoding $-\widehat{c}$ multiplied by a sign function translated to have origin at $r = R$), we can also write

(37)
$$C_0(\boldsymbol{x},r,t) = -\frac{2}{r}\sum_{n=1}^{\infty}(-1)^n e^{-\hat{D}(\hat{\mu}+a_n^2)t}\left(\frac{c_{\mathrm{init}}(\boldsymbol{x})}{a_n} + \hat{D}a_n\int_0^t \widehat{c}(\boldsymbol{x},\tau)e^{\hat{D}(\hat{\mu}+a_n^2)\tau}\,\mathrm{d}\tau\right)\sin a_n r,$$

where the boundary condition (35b) is now satisfied as $r\to R^-$.

Noting that $|\omega_m| = 1 - 4\pi R^3/3$ for spherical bacteria, we use (36) to write (34) as the homogenized equation

$$\frac{\partial\widehat{c}}{\partial t} = \nabla_{\boldsymbol{x}}\cdot\left(\left(1-\frac{4}{3}\pi R^3\right)\overline{D}(\boldsymbol{x})\nabla_{\boldsymbol{x}}\widehat{c}\right) - f[\widehat{c}], \tag{38a}$$

with the initial condition

$$\widehat{c}(\boldsymbol{x},0) = c_{\mathrm{init}}(\boldsymbol{x}), \tag{38b}$$

obtained by substituting (25e) into (6a), and where $f[\cdot]$ denotes that the effective uptake is a (nonlocal) functional, defined as

(38c)
$$f[\widehat{c}] = 8\pi R\hat{D}\sum_{n=1}^{\infty}\left\{e^{-\hat{D}(\hat{\mu}+a_n^2)t}\int_0^t\left(\frac{\partial\widehat{c}}{\partial\tau} + \hat{\mu}\hat{D}\widehat{c}(\boldsymbol{x},\tau)\right)e^{\hat{D}(\hat{\mu}+a_n^2)\tau}\,\mathrm{d}\tau\right\} - \frac{4}{3}\pi R^3\frac{\partial\widehat{c}}{\partial t}.$$

Thus, we have an effective integrodifferential equation for the leading-order intrinsic-averaged concentration. We note that the effective uptake is now significantly more complicated than for Case 1, and will depend on the initial conditions of the problem, but is still of $O(1)$.

We can also determine an equation for the volumetric-averaged concentration, defined in (6b), in terms of the intrinsic-averaged concentration. Substituting the asymptotic expansions (24) and leading-order solution (37) into the definition of the effective concentration (6b), we deduce that $\bar{c}$ can be calculated from $\widehat{c}$ using the relationship

(39)
$$\bar{c} \sim \left(1 - \frac{4}{3}\pi R^3\right)\widehat{c} + 8\pi R \sum_{n=1}^{\infty} e^{-\hat{D}(\hat{\mu}+a_n^2)t}\left(\frac{c_{\text{init}}(\boldsymbol{x})}{a_n^2} + \hat{D}\int_0^t \widehat{c}(\boldsymbol{x},s)e^{\hat{D}(\hat{\mu}+a_n^2)\tau}\,\mathrm{d}\tau\right).$$

For certain types of boundary conditions (e.g., Dirichlet, Robin, and mixed) on the boundary of Ω, it is possible to obtain a nontrivial steady solution to (38) and (39). It is simpler to analyze the effective uptake for Case 2 in the steady state than in the unsteady state, as the effective governing equation is reduced from an integrodifferential equation to the elliptic partial differential equation

$$0 = \nabla_{\boldsymbol{x}} \cdot \left(\left(1 - \frac{4}{3}\pi R^3\right)\overline{D}(\boldsymbol{x})\nabla_{\boldsymbol{x}}\widehat{c}\right) - \sigma\widehat{c}, \tag{40a}$$

where

$$\sigma = 4\pi R\hat{D}\left(\sqrt{\hat{\mu}}R\coth\sqrt{\hat{\mu}}R - 1\right), \tag{40b}$$

using the identity

$$\sum_{n=1}^{\infty}\frac{1}{\alpha + n^2\pi^2} = \frac{\sqrt{\alpha}\coth\sqrt{\alpha} - 1}{2\alpha}, \tag{41}$$

to reduce $f[\widehat{c}]$ to a linear function of $\widehat{c}$, in the steady state. We could also obtain (40a) by direct consideration of the steady version of (25). Additionally, we find that if $\widehat{c}$ tends to a constant as $t \to \infty$, (39) reduces to

$$\bar{c} \sim \left(1 - \frac{4}{3}\pi R^3\right)\widehat{c} + \frac{\sigma}{\hat{\mu}\hat{D}}\widehat{c}, \tag{42}$$

again using (41).

The steady state effective uptake coefficient in Case 2 is given by (40b). It is helpful to understand the sublimits of this coefficient in the steady regime before discussing the unsteady regime. For small $\sqrt{\hat{\mu}}R$, we see that

$$\sigma \sim \frac{4}{3}\pi\hat{\mu}\hat{D}R^3, \tag{43a}$$

the bacterium volume multiplied by the pointwise uptake rate within a bacterium. This volume scaling is the same effective uptake we derived in Case 1. For large $\sqrt{\hat{\mu}}R$, we deduce that

$$\sigma \sim 4\pi R\hat{D}(\sqrt{\hat{\mu}}R - 1) \sim 4\pi\sqrt{\hat{\mu}}\hat{D}R^2, \tag{43b}$$

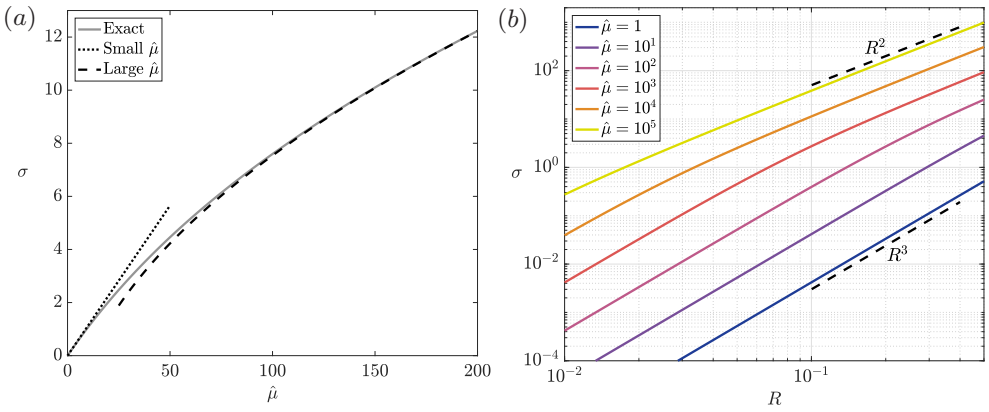

FIG. 3. *The steady state effective uptake coefficient σ in Case 2, given by* (40b) *as a function of* (a) $\hat{\mu}$ *(with $\hat{D} = 1$ and $R = 0.3$) and* (b) R *(with $\hat{D} = 1$). In* (a)*, we show that $\sigma \sim 4\pi R^3 \hat{D}\hat{\mu}/3$ for small $\hat{\mu}$ and $\sigma \sim 4\pi R\hat{D}(\sqrt{\hat{\mu}}R - 1)$ for large $\hat{\mu}$, as shown in* (43)*. In* (b)*, we show that σ scales with R^3 for small $\sqrt{\hat{\mu}}R$ and with R^2 for large $\sqrt{\hat{\mu}}R$.*

which is the product of the bacterium surface area, the pointwise uptake rate, and $1/\sqrt{\hat{\mu}}$, the width of an uptake boundary layer for large $\hat{\mu}$ near the bacterial membrane. Thus, the effective uptake function we have derived in (38c) provides the function that smoothly transitions between volume-scaled and surface-area-scaled effective bacterial uptake. We illustrate these results in Figure 3. We consider the generalization of these results to arbitrary bacterial shapes in Appendix A. In particular, we note that the physical intuition and subsequent scalings for the large pointwise uptake result given in (43b) generalizes for an arbitrary shape.

Although our main goal in this paper is to derive the effective uptake within a colony of bacteria, it is interesting to briefly consider $\hat{\mu} < 0$, corresponding to autocatalytic production of some chemical within the bacteria or positive autoregulation of gene expression. As $\hat{\mu}$ decreases, the steady state equation (40) yields a blow-up in the effective production rate when

$$\hat{\mu} = -\pi^2/R^2. \tag{44}$$

Thus, we may conclude that our steady state results are invalid for negative $\hat{\mu}$ when $\hat{\mu} \leq -\pi^2/R^2$. Additionally, although the chemical production is self-promoting in this scenario, a steady state is still possible when the above inequality is not satisfied.

In the unsteady regime, governed by the full homogenized system (38), we see that the effective uptake has a natural timescale of $O(1/\hat{D})$ for extreme values of $\hat{D}$. Thus, small and large $\hat{D}$ in (38) correspond to slow and fast uptake, respectively. In the limit of small $\hat{D}$, the leading-order intrinsic-averaged concentration becomes spatially independent over a timescale of $O(1/\hat{D})$, where the slow uptake is a function of time forced by (38c). The volumetric-averaged concentration is still given by the full form of (39). In the limit of large $\hat{D}$, the initial conditions quickly become unimportant and the effective uptake $f[\widehat{c}]$ reduces from a functional in $\widehat{c}$ to the linear function $\nu\widehat{c}$, defined in (40). This occurs because the fast diffusion removes the memory property from the upscaled problem. In the same manner, the volumetric-averaged concentration (39) tends to its steady state value (42) over a timescale of $O(1/\hat{D})$ in this limit. A

small $\hat{\mu}$ corresponds to slow uptake within the bacteria. In this limit, the unsteady concentration transport is governed by diffusion at leading order, before eventually tending to the small effective uptake given in (43a). A large $\hat{\mu}$ corresponds to quick uptake, and in this case the effective uptake $f[\widehat{c}]$ reduces from a functional in $\widehat{c}$ to the linear function $\nu\widehat{c}$, in the same manner as for large $\hat{D}$.

We note that taking the double limits of large $\hat{D}$ and small $\hat{\mu}$ commute, yielding an effective uptake of $4\pi R^3\hat{D}\hat{\mu}\widehat{c}/3$, which coincides with the effective uptake we derived in Case 1. Moreover, in the same limit, the upscaled governing equation (38) for Case 2 coincides with the upscaled governing equation (19) for Case 1, in the limit of D being small. Thus, we are able to smoothly pass between Cases 1 and 2, and, in fact, the effective uptake in Case 1 is a sublimit of the effective uptake in Case 2, and the effective diffusion in Case 2 is a sublimit of the effective diffusion in Case 1.

Each of the limiting results we discuss above could have been directly calculated by taking their respective limits before the homogenization procedure, but our method produces a distinguished limit from which the relevant sublimits can be distilled, as long as $R = O(1)$. In the next section, we consider the final distinguished limit, which occurs when R is small and μ is very large.

3.3. Case 3: Standard diffusion, very large uptake, and small bacterial size: $\boldsymbol{D = O(1)}$, $\boldsymbol{\mu = O(1/\epsilon^6)}$, $\boldsymbol{R = O(\epsilon^2)}$.

3.3.1. Asymptotic structure. We now consider the problem where $R \ll 1$ by investigating the distinguished limit $R = O(\epsilon^2)$, $\mu = O(1/\epsilon^6)$, and $D = O(1)$. Note that we have previously scaled R with the microscale variable, so in terms of dimensionless macroscale variables we are considering the case where the radius scales with the cube of the small parameter of periodicity, the critical case in [8]. We introduce $R = \epsilon^2\bar{R}$ and $\mu = \bar{\mu}/\epsilon^6$, where $\bar{R}$ and $\bar{\mu}$ are both of $O(1)$.

In this section, our analysis involves upscaling the governing equations (3) using a combination of boundary layer analysis and homogenization via the method of multiple scales. There are three important asymptotic regions in this problem. The first is the outer region, over which $\boldsymbol{x} = O(1)$. In the same manner as the previous two cases, we wish to determine an upscaled effective equation over this region that systematically accounts for the bacterial uptake. Thus, in the outer region, the bacterial uptake is a bulk effect. The second region is the cell region, over which $\boldsymbol{x} = O(\epsilon)$. This region will yield the cell problem, and, in this region, the bacterial uptake is a point sink. The third and final region is the inner region, over which $\boldsymbol{x} = O(\epsilon^3)$. In this region, we see the bacteria as an $O(1)$ region, within which we must solve a concentration problem coupled to the passive medium. The solution from the inner region determines the strength of the point sink in the cell region. Thus, this limit introduces an additional term to the previous equations (9) with which we worked. A schematic of these three regions is given in Figure 4.

3.3.2. Homogenization. Rewriting the equations (9) in terms of the scaled dimensionless parameters, we obtain

$$\epsilon^2\frac{\partial c}{\partial t} = (\nabla_{\boldsymbol{y}} + \epsilon\nabla_{\boldsymbol{x}})\cdot(\nabla_{\boldsymbol{y}} + \epsilon\nabla_{\boldsymbol{x}})\,c \quad \text{for } \|\boldsymbol{y}\| > \epsilon^2\bar{R} \text{ and } \|\boldsymbol{y}\|_\infty < 1/2, \tag{45a}$$

$$\epsilon^6\frac{\partial C}{\partial t} = \epsilon^4 D\,(\nabla_{\boldsymbol{y}} + \epsilon\nabla_{\boldsymbol{x}})\cdot(\nabla_{\boldsymbol{y}} + \epsilon\nabla_{\boldsymbol{x}})\,C - D\bar{\mu}C \quad \text{for } \|\boldsymbol{y}\| < \epsilon^2\bar{R}, \tag{45b}$$

$$c = C \quad \text{for } \|\boldsymbol{y}\| = \epsilon^2\bar{R}, \tag{45c}$$

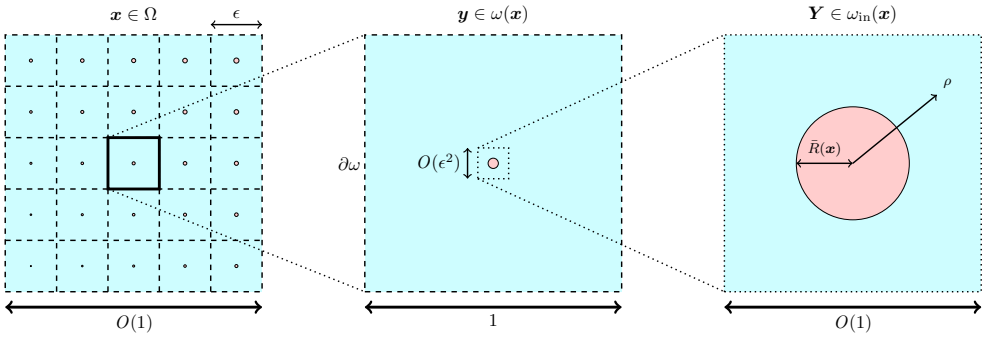

FIG. 4. *A two-dimensional projection of the asymptotic structure of the three-dimensional problem with small obstacles. The full problem is shown in the left figure, the center figure denotes the cell problem (with $\boldsymbol{y} \in [-1/2, 1/2]^3$), and the rightmost figure denotes the inner problem within the cell problem (with $\boldsymbol{Y} \in \mathbb{R}^3$ and $\rho = \|\boldsymbol{Y}\|$). In the cell problem, the effect of the bacterial sink occurs through a delta function, and not through its geometry. The strength of this sink is determined by solving the inner problem.*

(45d)
$$(\boldsymbol{n}_{\boldsymbol{y}} - \epsilon\nabla_{\boldsymbol{x}} R) \cdot (\nabla_{\boldsymbol{y}} + \epsilon\nabla_{\boldsymbol{x}})\, c = (\boldsymbol{n}_{\boldsymbol{y}} - \epsilon\nabla_{\boldsymbol{x}} R) \cdot D\,(\nabla_{\boldsymbol{y}} + \epsilon\nabla_{\boldsymbol{x}})\, C \quad \text{for } \|\boldsymbol{y}\| = \epsilon^2 \bar{R},$$

(45e)
$$c(\boldsymbol{x}, \boldsymbol{y}, 0) = c_{\text{init}}(\boldsymbol{x}) \quad \text{for } \|\boldsymbol{y}\| > \epsilon^2 \bar{R} \text{ and } \|\boldsymbol{y}\|_\infty < 1/2,$$

(45f)
$$C(\boldsymbol{x}, \boldsymbol{y}, 0) = c_{\text{init}}(\boldsymbol{x}) \quad \text{for } \|\boldsymbol{y}\| < \epsilon^2 \bar{R},$$

(45g)
$$c \text{ periodic} \quad \text{for } \|\boldsymbol{y}\|_\infty = 1/2.$$

We cannot obtain a solution for C by simply expanding in powers of ϵ, as we did for the previous two cases, since the bacterial domain in (45) depends on the small parameter ϵ. Instead, we seek an inner solution to the system near the small bacterium at the origin where $\|\boldsymbol{y}\| = O(\epsilon^2)$. In the next section, we show that the inner solution only affects the governing equation for c in the cell region at $O(\epsilon^2)$. Thus, substituting the asymptotic expansion $c(\boldsymbol{x}, \boldsymbol{y}, t) \sim c_0(\boldsymbol{x}, \boldsymbol{y}, t) + \epsilon c_1(\boldsymbol{x}, \boldsymbol{y}, t) + \epsilon^2 c_2(\boldsymbol{x}, \boldsymbol{y}, t)$ into (45a) implies that $c_0 = c_0(\boldsymbol{x}, t)$ and $c_1 = c_1(\boldsymbol{x}, t)$. We now investigate the inner region.

3.3.3. Inner region. We scale $\boldsymbol{y} = \epsilon^2 \boldsymbol{Y}$, where $\boldsymbol{Y} \in \mathbb{R}^3$. We define this inner region as $\omega_{\text{in}}(\boldsymbol{x})$, where the dependence on $\boldsymbol{x}$ arises from the radius of the bacterium in this domain. From (45), the relevant leading-order system is

(46a)
$$\nabla^2_{\boldsymbol{Y}} c = O(\epsilon^6) \quad \text{for } \rho > \bar{R}(\boldsymbol{x}),$$

(46b)
$$\nabla^2_{\boldsymbol{Y}} C - \bar{\mu} C = O(\epsilon^6) \quad \text{for } \rho < \bar{R}(\boldsymbol{x}),$$

(46c)
$$c = C \quad \text{for } \rho = \bar{R}(\boldsymbol{x}),$$

(46d)
$$\frac{\partial c}{\partial \rho} = D \frac{\partial C}{\partial \rho} + O(\epsilon^3) \quad \text{for } \rho = \bar{R}(\boldsymbol{x}),$$

(46e)
$$c \to c_0(\boldsymbol{x}, t) \quad \text{as } \rho \to \infty,$$

where $\rho = \|\boldsymbol{Y}\|$. The error estimate for (46d) arises from the slow variation in bacterium radius between neighboring cells, which will play no significant role in this analysis. The far-field condition (46e) arises from matching with the cell region using van Dyke's matching principle [29]. We do not require the initial conditions for this case as we are only concerned with the problem when $t = O(1)$.

Imposing a vanishing concentration flux at the origin to ensure boundedness, the general radially symmetric solution to (46) is

$$c = c_0(\boldsymbol{x},t)\left(1 - \frac{\bar{R}D}{\rho}\frac{\sqrt{\bar{\mu}}\bar{R}\coth\sqrt{\bar{\mu}}\bar{R} - 1}{1 + D\left(\sqrt{\bar{\mu}}\bar{R}\coth\sqrt{\bar{\mu}}\bar{R} - 1\right)}\right), \tag{47a}$$

$$C = \frac{c_0(\boldsymbol{x},t)\bar{R}\sinh\sqrt{\bar{\mu}}\rho}{\rho\left(D\sqrt{\bar{\mu}}\bar{R}\cosh\sqrt{\bar{\mu}}\bar{R} + (1-D)\sinh\sqrt{\bar{\mu}}\bar{R}\right)}. \tag{47b}$$

To correctly match into the cell region, we write the $O(1)$ solution in the inner region (47) in terms of the cell region variables and expand to $O(\epsilon^2)$, yielding

$$c \sim c_0(\boldsymbol{x},t) - \epsilon^2\frac{\nu}{4\pi\|\boldsymbol{y}\|}c_0(\boldsymbol{x},t), \tag{48}$$

where

$$\nu = \frac{4\pi\bar{R}D\left(\sqrt{\bar{\mu}}\bar{R}\coth\sqrt{\bar{\mu}}\bar{R} - 1\right)}{1 + D\left(\sqrt{\bar{\mu}}\bar{R}\coth\sqrt{\bar{\mu}}\bar{R} - 1\right)}. \tag{49}$$

The form of the matching condition (48) at $O(\epsilon^2)$ implies that the outer problem (45a) in the cell region with a boundary at $\|\boldsymbol{y}\| = \epsilon^2\bar{R}$ can be replaced by an effective outer problem in the cell region, replacing the small bacterial boundary with a Dirac delta function at the origin of strength $-\epsilon^2\nu c_0$. We now investigate this outer problem.

3.3.4. Higher-order cell region problem. Introducing the Dirac delta function formulation of the cell region problem (45), the $O(\epsilon^2)$ terms are

$$\frac{\partial c_0}{\partial t} = \nabla^2_{\boldsymbol{y}}c_2 + \nabla^2_{\boldsymbol{x}}c_0 - \nu\hat{\delta}(\boldsymbol{y})c_0 \quad \text{for } \boldsymbol{y}\in\omega, \tag{50a}$$

$$c_0 \text{ periodic} \quad \text{for } \boldsymbol{y}\in\partial\omega, \tag{50b}$$

where the introduction of a delta function is justified in the previous section.

Integrating (50a) over the cell, applying the periodic boundary conditions (50b), and noting that (6) yields $\widehat{c} \sim c_0$ at leading order, we obtain the effective equation for the intrinsic-averaged concentration

$$\frac{\partial\widehat{c}}{\partial t} = \nabla^2_{\boldsymbol{x}}\widehat{c} - \nu\widehat{c}, \tag{51a}$$

where ν is defined in (49), together with the initial condition

$$\widehat{c}(\boldsymbol{x},0) = c_{\text{init}}(\boldsymbol{x}), \tag{51b}$$

which arises by substituting (45e) into (6a). Moreover, as the bacteria are very small, with $|\omega_b| = O(\epsilon^2)$, the volumetric-averaged concentration $\bar{c} \sim \widehat{c}$, and thus (51) also provides the homogenized system for $\bar{c}$. As with the previous cases, the effective uptake is of $O(1)$, and for certain types of boundary conditions (e.g., Dirichlet, Robin, and mixed) on the boundary of Ω, it is possible to obtain a nontrivial steady solution to (51). The effective diffusion coefficient here is unity, and thus the effective diffusion in Case 3 is a sublimit of the effective diffusion in Case 1 as the bacterial radius becomes small.

The effective uptake in Case 3 is given by $\nu\widehat{c}$, defined in (49), and we now discuss how this scales with the bacterial properties. In a similar manner to Case 2, the parameter grouping $\sqrt{\bar{\mu}}\bar{R}$ is important. From (49), we see that a small $\sqrt{\bar{\mu}}\bar{R}$ yields

$$\nu \sim \frac{4}{3}\pi D\bar{\mu}\bar{R}^3, \tag{52}$$

which is the bacterium volume multiplied by the pointwise uptake rate within a bacterium. This is equivalent to (43a), the small uptake sublimit in Case 2, and thus is the same effective uptake we derived in Case 1. For a small D, we see from (49) that

$$\nu \sim 4\pi\bar{R}D\left(\sqrt{\bar{\mu}}\bar{R}\coth\sqrt{\bar{\mu}}\bar{R}-1\right), \tag{53}$$

which is equivalent to the steady state effective uptake coefficient σ from Case 2. This is because small D corresponds to bacteria that are much less permeable to the nutrient, the scenario considered in Case 2, and we have preserved the scaling $\epsilon^2\mu R^2 = O(1)$ in both Cases 2 and 3. For large $\sqrt{\bar{\mu}}\bar{R}$ or large D, we deduce that

$$\nu \sim 4\pi\bar{R}, \tag{54}$$

which, notably, is bounded above as $\bar{\mu} \to \infty$. This is because the nutrient concentration within each bacterium is much smaller in Case 3 than in Cases 1 and 2. Mathematically, for a large $\bar{\mu}$ in Case 3, the concentration within a bacterium is approximately $\widehat{c}/(D\sqrt{\bar{\mu}}\bar{R})$ near the bacterial membrane over a region depth of $O(1/\sqrt{\bar{\mu}})$ (see (47)), whereas for large $\hat{\mu}$ in nonsparse bacteria, as considered in section 3.2, the concentration within the bacterium scales with $\widehat{c}$ near the boundary over a region depth of $O(1/\sqrt{\hat{\mu}})$. Thus, the concentration within each bacterium is reduced as $\bar{\mu}$ gets larger, in a manner that bounds above the effective uptake. We show these scalings in Figure 5. We consider the generalization of these results to arbitrary bacterial shapes in Appendix A. We show that the effective uptake becomes independent of $\bar{\mu}$ as $\bar{\mu} \to \infty$, and we are also able to obtain analytic results for ellipsoidal bacteria in the same limit.

As with Case 2, it is interesting to briefly consider $\bar{\mu} < 0$ in Case 3, corresponding to autocatalytic production of some chemical or positive autoregulation of gene expression within the bacteria. As $\bar{\mu}$ decreases in this scenario, the effective production rate blows up in the homogenized equation (51) when

$$\sqrt{-\bar{\mu}}\bar{R}\cot\sqrt{-\bar{\mu}}\bar{R} = \frac{D-1}{D} \quad \text{for } \bar{\mu} \in \left(-\pi^2/\bar{R}^2, 0\right). \tag{55}$$

Thus, we may conclude that our homogenization results are invalid for negative $\bar{\mu}$ when $\bar{\mu}$ is less than the lower bound given by (55). We illustrate this lower bound in Figure 6. Moreover, as with Case 2, we note that although the chemical production is self-promoting in this scenario, a steady state is still possible provided that $-\bar{\mu}$ is not too large. This critical value depends on D, and we find that, as D increases, $-\bar{\mu}$ is restricted to smaller maximum values for our homogenization results to hold. We additionally note that (44), the blow-up in Case 2, is a sublimit of (55) for small D, with appropriate scalings of $\bar{\mu}$ and $\bar{R}$.

Finally, we note that we can formally pass between Cases 1, 2, and 3. We can smoothly pass between Cases 1 and 3 by considering the limits where $R \to 0$ and $\mu \to \infty$ with $\mu R^3 = O(1)$ in Case 1, and the limit where $\bar{R} \to \infty$ and $\bar{\mu} \to 0$ with $\bar{\mu}\bar{R}^3 = O(1)$ in Case 3. Additionally, we can smoothly pass between Cases 2 and 3 by

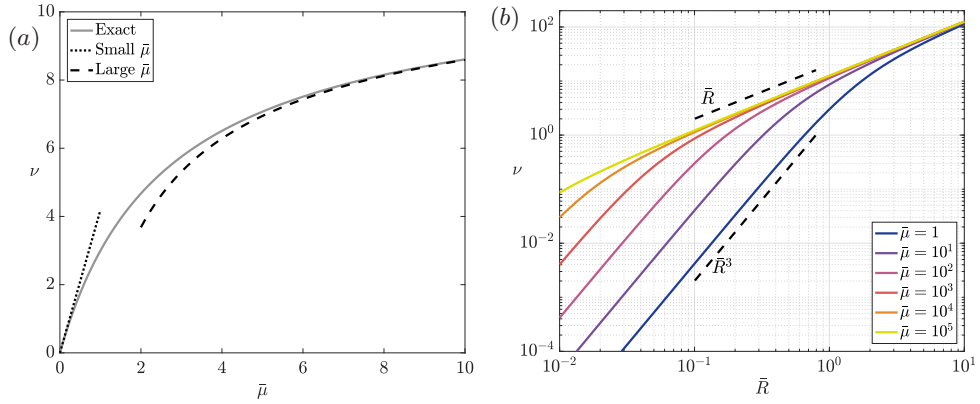

FIG. 5. *The effective uptake coefficient ν in Case 3, given by (49), as a function of* (a) $\bar{\mu}$ *(with $D = 1$ and $\bar{R} = 1$) and* (b) $\bar{R}$ *(with $D = 1$). In* (a)*, we show that $\nu \sim 4\pi\bar{R}^3 D\bar{\mu}/3$ for small $\bar{\mu}$ and $\nu \sim 4\pi\bar{R}(1 - 1/(\sqrt{\bar{\mu}}D\bar{R}))$ for large $\bar{\mu}$. In* (b)*, we show that ν scales with with $\bar{R}^3$ for small $\sqrt{\bar{\mu}}\bar{R}$ and with $\bar{R}$ for large $\sqrt{\bar{\mu}}\bar{R}$.*

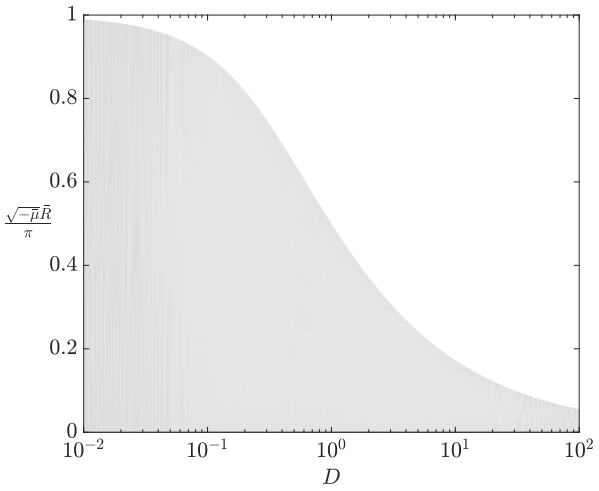

FIG. 6. *The gray region denotes the lower bound of the domain of validity for negative $\bar{\mu}$, which corresponds to autocatalytic production or positive autoregulation of gene expression within the bacteria. The boundary between domains is defined by* (55).

considering the limits where $R \to 0$ and $\hat{\mu} \to \infty$ with $\hat{\mu}R^2 = O(1)$ in Case 2, and the limit where $\bar{R} \to \infty$ and $D \to 0$ with $\bar{\mu}\bar{R}^2 = O(1)$ in Case 3. Thus, by considering the distinguished asymptotic limits, we have determined the different forms an $O(1)$ effective uptake can take over a timescale of $O(1)$, corresponding to the timescale of diffusion over the macroscale.

4. Discussion. We have systematically derived effective reaction–diffusion equations from the microscale problem of unsteady diffusion of nutrient through a passive medium containing a locally periodic array of spherical bacteria. The nutrient can diffuse within these bacteria, which also act as volume sinks of the nutrient with first-order kinetics. We have shown that with only two mechanisms, diffusion and uptake,

there are three distinguished limits where the effective uptake balances the macroscale diffusion over the timescale of the latter, and we have comprehensively investigated each limit. As we have investigated spherical bacteria, we have been able to maximize our analytic progress, and we have a closed-form expression for the effective uptake in each distinguished limit. We have been able to pass smoothly between each case as the system parameters vary, allowing us to determine how the effective uptake switches between scaling with the volume and surface area of the bacteria. Moreover, we have calculated the correct form of the effective uptake when neither of these scalings is correct.

While the effective uptake coefficients are our main focus in this paper, we have also determined effective diffusion coefficients for the upscaled problem. We briefly note that the important distinguished limit for the effective diffusion is given in Case 1; the effective diffusion coefficient in Case 2 is a sublimit of Case 1 as the pointwise diffusion coefficient within the bacteria vanishes, and the effective diffusion coefficient in Case 3 is a sublimit of Case 1 as the bacterial radius vanishes.

With regards to the effective uptake, the general behavior can be classified into two cases, depending on whether the typical bacterial radius is around the same size or much smaller than the distance between bacterial centers. When they are of the same order, the important distinguished limit occurs when the diffusion in the bacteria is small, in the double-porosity limit. This is Case 2, where there is a memory effect in the effective uptake, which is given as an explicit convolution of the nutrient concentration in terms of the system parameters in (38). Hence, the upscaling procedure converts a partial differential equation into an integrodifferential equation. This memory effect can fade over time to produce a valid steady equation, providing the external boundary conditions allow for this. In the steady case, the effective uptake becomes an explicit linear function of the instantaneous nutrient concentration, and we give an explicit result for the effective uptake coefficient σ in (40b). This explicit result shows how the effective uptake smoothly varies between scaling with bacterial volume and bacterial surface area, for a small and large reaction rate, respectively. In this manner, the effective uptake in Case 1 can be derived as a sublimit of σ as the pointwise diffusion coefficient within the bacteria becomes of the same order as the diffusion coefficient within the passive medium.

When the typical bacterial radius is much smaller than the distance between bacterial centers, the important distinguished limit occurs when the pointwise rate of nutrient uptake is large. This is Case 3, where we derive an explicit analytic expression for the effective uptake coefficient ν in (49). Notably, we find that ν is bounded above as the pointwise rate of nutrient uptake increases, and the supremum of this scales with the radii of the bacteria, as per the classic Smoluchowski result for uptake on the surface of a single sphere. Since ν also scales with the volume of the bacteria for a small pointwise uptake in this distinguished limit, we find that ν can scale from anywhere between the radius to the volume of the bacteria. In this manner, the effective uptake in Case 1 can be derived as a sublimit of ν as the pointwise uptake within the bacteria grows very large and the bacterial radius becomes of the same order as the distance between bacterial centers.

When mathematically modeling the nutrient uptake within a colony of growing bacteria, one may derive and investigate a governing equation in terms of the bacterial volume. In this paper, we have provided the correct uptake terms for such an equation in terms of the bacterial properties. Even though we start from a linear pointwise uptake, our work shows that the effective uptake should only scale linearly with the bacterial volume under certain circumstances, notably when the pointwise uptake is

very weak. Otherwise, the effective uptake can scale with, for example, the bacterial surface area or radius, and the uptake should thus be a nonlinear function of the bacterial volume.

Although the main goal of this paper is to determine the effective uptake within a colony of bacteria, by considering a negative uptake coefficient (corresponding to a positive production coefficient) our results can be modified to investigate autocatalytic production of some chemical or positive autoregulation of gene expression within the bacteria. Our homogenized equations are still valid as the uptake coefficient decreases through zero, but we show that the effective production rate will blow up when the production coefficient reaches a critical value defined by (55) in Case 3. The corresponding result for Case 2 is a sublimit of the Case 3 result, when the diffusion coefficient within the bacteria becomes much smaller than within the passive medium. Since the dominant balance in the asymptotic scalings will change close to this apparent blow-up, it would be interesting to investigate the blow-up problem of autocatalytic production in more detail.

As the leading-order concentration within the passive medium does not depend on the microscale variable in all the cases we consider, we expect our effective uptake results to hold for any Bravais lattice of spheres, with an appropriate scaling to account for the relative volumes of the bacterial phase and the (locally) periodic cell. However, the effective diffusion coefficients will not translate directly, as the geometry of the cell problem will change. Our work in Case 1 can be applied directly to more general arrays of spheres, and the relevant effective diffusion coefficients can be obtained from (19c) by solving the cell problem (15) for different arrays. Additionally, in this paper we have modeled the spatial variation in bacterial density by allowing the bacterial radius to vary slowly in space. Another way to model this change in bacterial density is to consider a slow variation in the lattice on which the bacterial centers lie—that is, to consider a locally periodic lattice that varies slowly in space and use the methods of [26] to transform this near-periodic microscale to a strictly periodic microscale. As shown in [5], if we use a conformal transformation to preserve the spherical shape of the bacteria, the nature of the Jacobian matrix of the transformation would result in a greatly simplified cell problem for the diffusion coefficient. Moreover, as the transformation only affects spatial derivatives, we would still expect our results for the effective uptake to apply after the transformation. In this paper we have not considered the problem of large pointwise uptake when the typical bacterial radius is around the same size as the distance between bacterial centers. In such a case, the uptake timescale would be much quicker than the timescale of diffusion over the bioreactor lengthscale, yielding large depleted regions within the passive medium, and the nutrient uptake would be localized to boundary layers near the bacterial membrane.

We have used initial conditions that are continuous across the bacterial membrane and allow for a slow variation in the concentration over the bioreactor lengthscale. Although these initial conditions are idealized, the initial conditions of the system are only significant in Case 2. Moreover, in Case 2 the effect of the initial conditions decays over time. For more general initial conditions, we will have early-time boundary layers where the initial conditions settle down. In Case 1, general initial conditions will settle over a timescale of $t = O(\epsilon^2)$ to the conditions we use in this paper. In Case 2, general initial conditions within the passive medium will become independent of the short bacterial lengthscale over the same timescale, but the initial conditions within the bacteria will only decay over a timescale of $t = O(1)$. In Case 3, general initial conditions within the bacteria will settle to the steady state solution over a

timescale of $t = O(\epsilon^6)$, whereas general initial conditions within the passive medium will settle over a timescale of $t = O(\epsilon^2)$.

In this paper we mainly consider bacteria with a spherical morphology, known as *cocci*. Although this is a common morphology, there are other possible bacterial shapes, ranging from the more prevalent rod-shaped (*bacilli*) to the more unusual star-shaped (*stella*). In Appendix A we discuss the generalization of our results to arbitrary bacterial shapes, and we provide the systems that would have to be solved to obtain the upscaled results for a given bacterial shape. Although explicit analytic results are only possible in certain circumstances, the distinguished limits we discuss in this paper provide the important scalings for arbitrary bacterial shapes under the uptake form and coupling conditions we consider. Notably, in the limit of large pointwise uptake in Case 3, we are able to obtain closed-form solutions for the effective uptake by ellipsoidal bacteria in terms of the incomplete elliptic integral of the first kind.

There are several further natural extensions to the work in this paper. For example, we have neglected the role of advective transport in this model, allowing us to focus on the three distinguished limits that arise with just diffusion and uptake as the transport processes. The inclusion of advection would present more distinguished limits in the system, and these could be explored by using the results in this paper as a basis from which to extend. Another simplifying assumption we make is that the uptake reaction has first-order kinetics. This results in a linear uptake term in the cell problem, facilitating our analytic solutions to the cell problems and yielding explicit terms for the effective uptake. This uptake term could be generalized to different nonlinear reaction terms, such as Michaelis–Menten or Freundlich-type uptake terms, and it may not be possible to obtain explicit analytic results for these cases.

We have neglected any internal structure of the bacteria, as we have assumed that the bacterial phases are homogeneous. Moreover, we have assumed a unit partition coefficient between the bacteria and the passive medium, as we took continuity of concentration through the bacterial membrane. It would be simple to modify the analytic results in this paper to account for a nonunit partition coefficient between the interior and exterior of the bacteria. If there were specific problems that required nonlinear coupling conditions or an inhomogeneous internal structure to be included, the framework we have developed in this paper could be extended to include such properties, but analytic results are unlikely. With recent advances in high-resolution imaging techniques for bacteria, such as those used in [13], one could develop a more accurate model of the bacterial interior and use experimentally relevant bacterial shapes and distributions of bacteria, allowing the upscaling procedure to be performed on a more accurate description of the microstructure.

In this paper, we have investigated and quantified how the effective uptake scales with bacterial properties such as size, diffusivity, and pointwise uptake. We have shown when it is valid to scale the effective uptake with the bacterial volume, when scaling with the surface area is more appropriate, how to transition between these two scalings, and how to identify and deal with the case when neither scaling is correct. Moreover, the diffusion–reaction system we consider is not just limited to bacteria; it can also be applied to other single-celled microorganisms, such as cyanobacteria, microalgae, protozoa, and yeast. More generally, solute transport problems are nearly ubiquitous in applied mathematics, and the framework of this paper can be extended to consider other particular problems. We hope that our systematic upscaling results will be used to impose accurate effective uptake rates for general models of solute

uptake in as wide a range of physical areas as possible.

Appendix A. General-shaped bacteria. In this appendix, we consider some generalizations of our results to nonspherical bacteria, in part to emphasize the broader applicability of the above methodologies. For notational brevity, we still refer to the bacterial and medium domains as $\omega_b(\boldsymbol{x})$ and $\omega_m(\boldsymbol{x})$, respectively. For Case 1, it is simple to deduce that (19a), the effective governing equation, becomes

$$\frac{\partial \widehat{c}}{\partial t} = \nabla_{\boldsymbol{x}} \cdot (\mathbf{D}(\boldsymbol{x}) \nabla_{\boldsymbol{x}} \widehat{c}) - \mu |\omega_b(\boldsymbol{x})| \widehat{c}, \tag{A1}$$

where $\mathbf{D}$ is a tensor equal to the right-hand side of (19c), requiring solutions to the cell problem (15) with arbitrary bacterial and medium domains.

For Case 2, the effective governing equations are still given by (34)–(35), but we note that it is difficult to give an analytic solution to (35) for a general-shaped bacterial domain. However, for a large pointwise uptake coefficient, $\hat{\mu} \gg 1$, the majority of the uptake is located in a boundary layer close to the bacterial membrane. To determine the concentration within this boundary layer, it is convenient to work in a general curvilinear coordinate system with n denoting the direction normal to the membrane such that $n = 0$ on the bacterial membrane, with $n > 0$ corresponding to the passive medium and $n < 0$ corresponding to the bacterial domain. Then, in the limit $\hat{\mu} \gg 1$, the asymptotic solution to (35) is

$$C_0 \sim \widehat{c}(\boldsymbol{x}, t) e^{\hat{\mu}^{1/2} n}. \tag{A2}$$

Using this result in (34), the effective governing equation for the intrinsic-averaged concentration for general-shaped bacteria is

$$|\omega_m(\boldsymbol{x})| \frac{\partial \widehat{c}}{\partial t} = \nabla_{\boldsymbol{x}} \cdot \left(|\omega_m(\boldsymbol{x})| \overline{D}(\boldsymbol{x}) \nabla_{\boldsymbol{x}} \widehat{c} \right) - \hat{\mu}^{1/2} \hat{D} |\partial \omega_b(\boldsymbol{x})| \widehat{c}. \tag{A3}$$

This result generalizes the large $\hat{\mu}$ result for *cocci* that we derived in (43b) for the steady state, showing that the effective uptake coefficient is the product of the pointwise uptake $\hat{\mu}\hat{D}$, the width of the boundary layer within a bacterium $\hat{\mu}^{-1/2}$, and the surface area of the bacteria $|\partial \omega_b(\boldsymbol{x})|$. Noting that the volumetric-averaged concentration $\bar{c} = |\omega_m(\boldsymbol{x})| \widehat{c} + O(\hat{\mu}^{-1/2})$ for large $\hat{\mu}$, we can also write the following effective governing equation for the volumetric-averaged concentration with general-shaped bacteria:

$$\frac{\partial \bar{c}}{\partial t} = \nabla_{\boldsymbol{x}} \cdot \left(\overline{D}(\boldsymbol{x}) \nabla_{\boldsymbol{x}} \bar{c} - \frac{\nabla_{\boldsymbol{x}} |\omega_m(\boldsymbol{x})|}{|\omega_m(\boldsymbol{x})|} \bar{c} \right) - \hat{\mu}^{1/2} \hat{D} \frac{|\partial \omega_b(\boldsymbol{x})|}{|\omega_m(\boldsymbol{x})|} \bar{c}. \tag{A4}$$

Here, we note the appearance of an effective advection term which arises due to spatial variation in bacterial volume, as expected for diffusion past impermeable obstacles [5]. Additionally, we note that the effective uptake in (A4) has an equivalent geometrical dependence to the effective uptake in the simpler (single-phase) problem with partial adsorption on the surface of obstacles arranged in a periodic array. This single-phase case is considered in [10, 11] and is a similar but reduced version of the problem considered in this paper, as the concentration evolution within the bacterial/obstacle phase is not considered. To obtain the model in [10, 11], the dimensional governing equation (2b) and interfacial conditions (2c,d) should be replaced with the dimensional boundary condition

$$\boldsymbol{n} \cdot D_m \nabla \tilde{c} = -\gamma \tilde{c} \quad \text{for } \tilde{\boldsymbol{x}} \in \partial \Omega_b. \tag{A5}$$

Comparing the effective uptake results for surface adsorption in [10, 11] with the effective uptake for volume sinks with large pointwise coefficient in (A4), we deduce that an equivalent effective uptake is obtained when $\gamma = (\lambda D_b)^{1/2}$, recalling that λ is the dimensional volume uptake coefficient in this paper.

To generalize Case 3, we redefine the bacterial domain in the inner domain using $\overline{\omega_b}(\boldsymbol{x})$ instead of $\omega_b(\boldsymbol{x})$, where $|\omega_b| = \epsilon^6|\overline{\omega_b}|$ and $|\overline{\omega_b}| = O(1)$. For the spherical case in section 3.3, this volume scaling is implied by the radial scaling $R = \epsilon^2\bar{R}$.

Then, using the scaling $\boldsymbol{y} = \epsilon^2\boldsymbol{Y}$, the leading-order system (46) becomes

$$\nabla^2_{\boldsymbol{Y}} c = 0 \quad \text{for } \boldsymbol{Y} \in \mathbb{R}^3 \setminus \overline{\omega_b}(\boldsymbol{x}), \tag{A6a}$$

$$\nabla^2_{\boldsymbol{Y}} C - \bar{\mu} C = 0 \quad \text{for } \boldsymbol{Y} \in \overline{\omega_b}(\boldsymbol{x}), \tag{A6b}$$

$$c = C \quad \text{for } \boldsymbol{Y} \in \partial\overline{\omega_b}(\boldsymbol{x}), \tag{A6c}$$

$$\frac{\partial c}{\partial n} = D\frac{\partial C}{\partial n} \quad \text{for } \boldsymbol{Y} \in \partial\overline{\omega_b}(\boldsymbol{x}), \tag{A6d}$$

$$c \to c_0(\boldsymbol{x}, t) \quad \text{as } |\boldsymbol{Y}| \to \infty. \tag{A6e}$$

The effective governing equation is then given by (51), using

$$\nu = \frac{1}{c_0(\boldsymbol{x}, t)} \int_{\partial\overline{\omega_b}(\boldsymbol{x})} \frac{\partial c}{\partial n} \, \mathrm{d}s, \tag{A7}$$

where $\mathrm{d}s$ denotes a surface element of the bacterial membrane and c is a solution to the coupled system (A6). As with the generalized Case 2, we are unable to solve (A6) analytically for a general-shaped bacterial domain. We are able to make further analytic progress in the limit of large $\bar{\mu}$, when the problems in each phase decouple from one another. In this case, there is a boundary layer within each bacterium near the bacterial membrane, where the concentration decreases exponentially with argument $\sqrt{\bar{\mu}}n$, in a similar manner to (A2). However, the prefactor of this exponential is not known a priori and must be determined by solving the decoupled system for c, given by

$$\nabla^2_{\boldsymbol{Y}} c = 0 \quad \text{for } \boldsymbol{Y} \in \mathbb{R}^3 \setminus \overline{\omega_b}(\boldsymbol{x}), \tag{A8a}$$

$$c = 0 \quad \text{for } \boldsymbol{Y} \in \partial\overline{\omega_b}(\boldsymbol{x}), \tag{A8b}$$

$$c \to c_0(\boldsymbol{x}, t) \quad \text{as } |\boldsymbol{Y}| \to \infty. \tag{A8c}$$

Thus, from (A7) we see that the effective uptake coefficient can be determined by solving (A8) and, notably, we see that the effective uptake coefficient is independent of $\bar{\mu}$ and D in the large $\bar{\mu}$ limit.

We may obtain an analytic expression for the solution to (A8), and hence the effective uptake coefficient, for ellipsoidal bacteria, exploiting the separability of the Laplace operator in ellipsoidal coordinates.[1] For brevity, we consider a strictly periodic array of bacteria, define the longest semi-axis to have length $\bar{R}$, and scale $\boldsymbol{Y} = \bar{R}\bar{\boldsymbol{Y}}$, such that the bacterial region in one periodic cell is defined as

$$\overline{\omega_b} := \left\{ \bar{\boldsymbol{Y}} \in \mathbb{R}^3 : \bar{Y}_1^2 + \frac{\bar{Y}_2^2}{\alpha^2} + \frac{\bar{Y}_3^2}{\beta^2} < 1 \right\}. \tag{A9}$$

[1] We note that a similar geometry in (A6) would also be analytically tractable, as the Helmholtz operator is also separable in ellipsoidal coordinates, but this is beyond the scope of this paper.

Here, $\bar{Y}_i$ for $i = 1, 2, 3$ are three Cartesian components of $\bar{\boldsymbol{Y}}$. Without loss of generality, we are able to orient these axes to coincide with the semi-axes of the ellipsoidal bacteria; on the lengthscale of the homogenization cell, the apparent point sink from bacterial uptake has no preferred angle. Additionally, the two constants α and β satisfy $0 < \beta \leqslant \alpha \leqslant 1$, again without loss of generality. Spherical bacteria are obtained when $\alpha = \beta = 1$. By transforming to ellipsoidal coordinates, the solution to (A8) can be written as

$$c = c_0(\boldsymbol{x}, t)\left(1 - \frac{F\left(\frac{\sqrt{1-\beta^2}}{\zeta(\bar{\boldsymbol{Y}})}; \sqrt{\frac{1-\alpha^2}{1-\beta^2}}\right)}{F\left(\sqrt{1-\beta^2}; \sqrt{\frac{1-\alpha^2}{1-\beta^2}}\right)}\right), \tag{A10}$$

where

$$F(x; k) = \int_0^x \frac{\mathrm{d}s}{\sqrt{(1-s^2)\,(1-k^2 s^2)}} \tag{A11}$$

is the incomplete elliptic integral of the first kind.[2] Here, $\zeta^2(\bar{\boldsymbol{Y}})$ is defined as the solution to the following cubic in ζ^2:

$$\frac{\bar{Y}_1^2}{\zeta^2} + \frac{\bar{Y}_2^2}{\zeta^2 + \alpha^2 - 1} + \frac{\bar{Y}_3^2}{\zeta^2 + \beta^2 - 1} = 1, \tag{A12}$$

where $\zeta(\bar{\boldsymbol{Y}}) \geqslant 1$, with equality defining the ellipsoidal surface. Rather than directly evaluating (A7) to determine the effective uptake, it is simpler to expand (A10) in the large ζ limit, accounting for the scaling $\boldsymbol{Y} = \bar{R}\bar{\boldsymbol{Y}}$, and then use the divergence theorem to deduce that

$$\nu = \frac{4\pi\bar{R}\sqrt{1-\beta^2}}{F\left(\sqrt{1-\beta^2}; \sqrt{\frac{1-\alpha^2}{1-\beta^2}}\right)}. \tag{A13}$$

We show how ν varies with α and β in Figure 7. Of particular interest are the subcases of oblate and prolate spheroids, being plausible geometries for some bacteria. An oblate spheroid corresponds to $\alpha = 1$ with $\beta < 1$, resulting in an effective uptake

$$\nu = \frac{4\pi\bar{R}\sqrt{1-\beta^2}}{\sin^{-1}\sqrt{1-\beta^2}}. \tag{A14}$$

A prolate spheroid corresponds to $\alpha = \beta < 1$, resulting in an effective uptake

$$\nu = \frac{4\pi\bar{R}\sqrt{1-\beta^2}}{\tanh^{-1}\sqrt{1-\beta^2}}. \tag{A15}$$

As bacilli or coccobacilli can be modeled as prolate spheroids, (A15) gives the effective uptake through either such colony in the limits of large pointwise uptake and large

[2]We give (A11) in Jacobi's form here for notational purposes, though we note that the trigonometric form is more amenable to numerical calculation when $\beta \to 0$ and thus when $x \to 1$ in (A11).

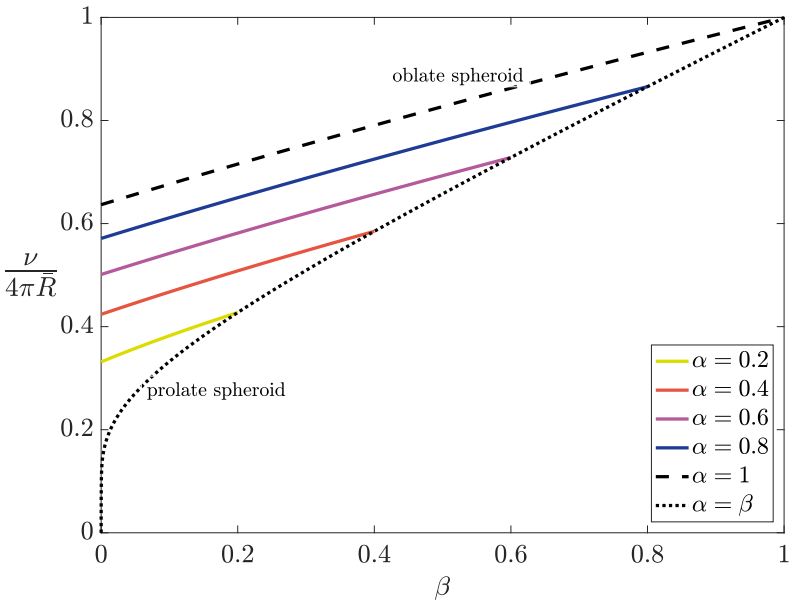

FIG. 7. *The normalized effective uptake, $\nu/(4\pi\bar{R})$, for small ellipsoidal bacteria in the limit of large uptake, as given in* (A13). *The principal semi-axes have lengths $\bar{R}$, $\alpha\bar{R}$, and $\beta\bar{R}$, where $0 < \beta \leqslant \alpha \leqslant 1$. The case where $\alpha = 1$ corresponds to an oblate spheroid, and the case where $\alpha = \beta$ corresponds to a prolate spheroid.*

separation between bacteria. Additionally, in the limit of $\beta \to 0$, we note that the effective uptake is finite for $\alpha > 0$ (where the bacteria is a two-dimensional disk) but vanishes with a logarithmic dependence when we also consider $\alpha \to 0$ (where the bacteria is a one-dimensional rod). Thus, long thin bacteria with a large separation distance will have a negligible effect on removing nutrient from the system, even when their pointwise uptake is very large. We also note that in the special case of spherical bacteria, attained in the limits $\alpha \to 1$ and $\beta \to 1$, the effective uptake reduces to that of (54), as expected.

REFERENCES

[1] T. ARBOGAST, J. DOUGLAS, JR., AND U. HORNUNG, *Derivation of the double porosity model of single phase flow via homogenization theory*, SIAM J. Math. Anal., 21 (1990), pp. 823–836, https://doi.org/10.1137/0521046.

[2] A. G. BELYAEV, A. L. PYATNITSKII, AND G. A. CHECHKIN, *Asymptotic behavior of a solution to a boundary value problem in a perforated domain with oscillating boundary*, Siberian Math. J., 39 (1998), pp. 621–644, https://doi.org/10.1007/BF02673049.

[3] A. BENSOUSSAN, J.-L. LIONS, AND G. PAPANICOLAOU, *Asymptotic Analysis for Periodic Structures*, North–Holland, Amsterdam, 1978.

[4] R. B. BIRD, W. E. STEWART, AND E. N. LIGHTFOOT, *Transport Phenomena*, John Wiley & Sons, New York, 2007.

[5] M. BRUNA AND S. J. CHAPMAN, *Diffusion in spatially varying porous media*, SIAM J. Appl. Math., 75 (2015), pp. 1648–1674, https://doi.org/10.1137/141001834.

[6] S. J. CHAPMAN, D. P. HEWETT, AND L. N. TREFETHEN, *Mathematics of the Faraday cage*, SIAM Rev., 57 (2015), pp. 398–417, https://doi.org/10.1137/140984452.

[7] G. A. CHECHKIN AND A. L. PIATNITSKI, *Homogenization of boundary-value problem in a locally periodic perforated domain*, Appl. Anal., 71 (1998), pp. 215–235, https://doi.org/10.1080/00036819908840714.

[8] D. Cioranescu and F. Murat, *A strange term coming from nowhere*, in Topics in the Mathematical Modelling of Composite Materials, Springer, New York, 1997, pp. 45–93, https://doi.org/10.1007/978-1-4612-2032-9_4.
[9] C. Conca, A. Liñán, and C. Timofte, *Homogenization in chemical reactive flows*, Electron. J. Differential Equations, 40 (2004), pp. 1–22.
[10] M. P. Dalwadi, M. Bruna, and I. M. Griffiths, *A multiscale method to calculate filter blockage*, J. Fluid Mech., 809 (2016), pp. 264–289, https://doi.org/10.1017/jfm.2016.656.
[11] M. P. Dalwadi, I. M. Griffiths, and M. Bruna, *Understanding how porosity gradients can make a better filter using homogenization theory*, Proc. A, 471 (2015), 20150464, https://doi.org/10.1098/rspa.2015.0464.
[12] Y. Davit, C. G. Bell, H. M. Byrne, L. A. C. Chapman, L. S. Kimpton, G. E. Lang, K. H. L. Leonard, J. M. Oliver, N. C. Pearson, R. J. Shipley, S. L. Waters, J. P. Whiteley, B. D. Wood, and M. Quintard, *Homogenization via formal multiscale asymptotics and volume averaging: How do the two techniques compare?*, Adv. Water Res., 62 (2013), pp. 178–206, https://doi.org/10.1016/j.advwatres.2013.09.006.
[13] K. Drescher, J. Dunkel, C. D. Nadell, S. van Teeffelen, I. Grnja, N. S. Wingreen, H. A. Stone, and B. L. Bassler, *Architectural transitions in* Vibrio cholerae *biofilms at single-cell resolution*, Proc. Natl. Acad. Sci. USA, 113 (2016), pp. E2066–E2072, https://doi.org/10.1073/pnas.1601702113.
[14] T. Fatima, N. Arab, E. P. Zemskov, and A. Muntean, *Homogenization of a reaction–diffusion system modeling sulfate corrosion of concrete in locally periodic perforated domains*, J. Engrg. Math., 69 (2011), pp. 261–276, https://doi.org/10.1007/s10665-010-9396-6.
[15] M. Gahn, M. Neuss-Radu, and P. Knabner, *Homogenization of reaction–diffusion processes in a two-component porous medium with nonlinear flux conditions at the interface*, SIAM J. Appl. Math., 76 (2016), pp. 1819–1843, https://doi.org/10.1137/15M1018484.
[16] M. H. Holmes, *Introduction to Perturbation Methods*, Texts Appl. Math. 20, Springer-Verlag, New York, 2013.
[17] U. Hornung, ed., *Homogenization and Porous Media*, Interdiscip. Appl. Math. 6, Springer-Verlag, New York, 1997.
[18] U. Hornung, W. Jäger, and A. Mikelić, *Reactive transport through an array of cells with semi-permeable membranes*, Math. Model. Numer. Anal., 28 (1994), pp. 59–94.
[19] V. V. Jikov, S. M. Kozlov, and O. A. Oleinik, *Homogenization of Differential Operators and Integral Functionals*, Springer-Verlag, Berlin, 1994.
[20] J. D. Keasling, *Manufacturing molecules through metabolic engineering*, Science, 330 (2010), pp. 1355–1358, https://doi.org/10.1126/science.1193990.
[21] P. A. Levin and E. R. Angert, *Small but mighty: Cell size and bacteria*, Cold Spring Harbor Perspec. Biol., 7 (2015), a019216, https://doi.org/10.1101/cshperspect.a019216.
[22] H. Märkl, C. Zenneck, A. C. H. Dubach, and J. C. Ogbonna, *Cultivation of Escherichia coli to high cell densities in a dialysis reactor*, Appl. Microbiol. Biotech., 39 (1993), pp. 48–52, https://doi.org/10.1007/BF00166847.
[23] F. Murat and D. Cioranescu, *Un terme étrange venu d'ailleurs*, in Nonlinear Partial Differential Equations and Their Applications, Volumes II and III, Collége de France Seminar, Paris, France, 1982, pp. 98–138.
[24] M. Panfilov, *Macroscale Models of Flow through Highly Heterogeneous Porous Media*, Theory Appl. Transport Porous Media 16, Springer, Dordrecht, The Netherlands, 2000.
[25] N. Ray, T. Elbinger, and P. Knabner, *Upscaling the flow and transport in an evolving porous medium with general interaction potentials*, SIAM J. Appl. Math., 75 (2015), pp. 2170–2192, https://doi.org/10.1137/140990292.
[26] G. Richardson and S. J. Chapman, *Derivation of the bidomain equations for a beating heart with a general microstructure*, SIAM J. Appl. Math., 71 (2011), pp. 657–675, https://doi.org/10.1137/090777165.
[27] E. Sánchez-Palencia, *Non-Homogeneous Media and Vibration Theory*, Lecture Notes in Phys. 127, Springer-Verlag, Berlin, 1980.
[28] R. J. Shipley and S. J. Chapman, *Multiscale modelling of fluid and drug transport in vascular tumours*, Bull. Math. Biol., 72 (2010), pp. 1464–1491, https://doi.org/10.1007/s11538-010-9504-9.
[29] M. van Dyke, *Perturbation Methods in Fluid Dynamics*, Parabolic Press, Stanford, CA, 1975.
[30] T. L. van Noorden, *Crystal precipitation and dissolution in a porous medium: Effective equations and numerical experiments*, Multiscale Model. Simul., 7 (2009), pp. 1220–1236, https://doi.org/10.1137/080722096.

[31] T. L. van Noorden and A. Muntean, *Homogenisation of a locally periodic medium with areas of low and high diffusivity*, European J. Appl. Math., 22 (2011), pp. 493–516, https://doi.org/10.1017/S0956792511000209.
[32] S. Whitaker, *The Method of Volume Averaging*, Theory Appl. Transport Porous Media 13, Springer, Dordrecht, The Netherlands, 1999.